Compressive behaviour of confined polycrystalline ice

Barrette, Paul; Jordaan, I.

Publisher's version / Version de l'éditeur:
https://doi.org/10.4224/12340921
PERD/CHC report, 2001-12

Memorial
University of Newfoundland

PERD

Compressive Behaviour
Of Confined Polycrystalline Ice

Report

prepared for

The National Research Council
Program on Energy Research and Development (PERD)

By

Paul D. Barrette and Ian J. Jordaan
Ocean Engineering Research Centre
Memorial University of Newfoundland
St. John's, NF

December 2001

PERD/CHC REPORT 4-77

Table of Content

Acknowledgements

The experimental work presented in this report was done with the assistance of several COOP work-term students registered in the Engineering program of Memorial University of Newfoundland. These are: Amanda Bromley, Sterling Parsons, Paul Garnier and Thomas Mackey. Ron O'Driscoll and Austin Bursey, both technicians at the Faculty of Engineering and Applied Science, looked after the maintenance of the cold room refrigeration unit and the MTS hydraulic system. Austin Bugden, technical officer with the Institute for Marine Dynamics (IMD) of the National Research Council of Canada in St.John's, endeavoured to accommodate our needs for the IMD cold room facility and its ice machining and thin sectioning equipment.

Dr. Irene Meglis collaborated with the data production in the early stages of the project. She was instrumental in gathering an initial database. Both Dr. Meglis and Paul Melanson provided useful guidance in initiating the ice production procedure and setting up the MTS system to resume ice testing.

Dr. Stephen Jones allowed us access to IMD and the logistical support that was necessary to carry out the research presented in this report. Dr. Jones also made his expertise available in a number of discussions on the interpretation of the data.

1. Introduction

The design of structures and vessels for arctic and subarctic waters requires knowledge of ice loads and their distribution in space and time. This in turn requires analyses of the interaction between the structure and the ice at conditions that are representative of the real scale event (displacement rate, confining pressure, deviatoric stress, temperature). Medium-scale field investigations have been carried out in the past in an effort to better comprehend the failure processes in the ice during these interactions. An example of this are a series of indentation tests that have been conducted with iceberg and multiyear ice (Frederking et al. 1990, Masterson et al. 1992, 1999). A test set-up is shown in Figure 1.

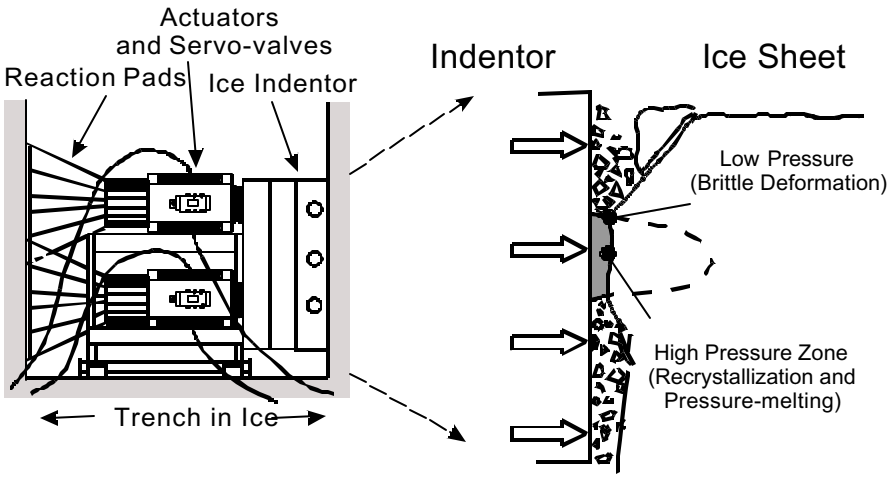

Figure 1: Medium-scale field testing experiments.

Indentors of various shapes were used. Loads, displacements and temperature are some of the parameters that were recorded during these tests. The actuator response typically displayed a saw-tooth loading pattern that was explained by the dynamics of the failure processes occurring in the ice. Local pressures along the interface between the ice and the structure reach relatively high levels (up to 70 MPa, according to Frederking et al. 1990). Our analyses of the medium-scale field events produced with either iceberg or multiyear ice has outlined non-simultaneous failure modes and the occurrence of high pressure zones that effectively control the load applied onto the structure (Jordaan et al. 1999, 2001)(Fig. 1). Mechanisms of a ductile nature, such as recrystallization, have been shown to occur in these zones (Muggeridge and Jordaan 1999). The brittle behaviour and spalling accompanying ice failure are closely associated with what is happening inside the high pressure zones. An adequate representation of the deformation mechanisms occurring in the ice during mechanical testing therefore requires high confinement levels.

Triaxial testing was done by a number of investigators. Amongst the most interesting observations made in some of these studies is an increase followed by a decrease in strength of the material with an increase in confinement, particularly at high strain rates

(Jones 1978, 1982, Nadreau and Michel 1986, Richter-Menge 1991, Mizuno 1998). A decrease followed by an increase of 'compliance' with an increase in confinement was also reported in constant load tests (Jones and Chew 1983, Melanson et al. 1999a, Barrette and Jordaan 2001). This reversal in trend, if representative of what is taking place during a real ice-structure interaction, is significant for two reasons:

First, it indicates that high-pressure zones may become 'softer' where pressure is highest, thereby exerting some control on the failure mode of these zones and the resulting load-unloading cycles.

Second, the reason for this reversal was attributed to recrystallization phenomena and the pressure melting of ice. Evidence of these mechanisms was provided (Frederking et al. 1990, Gagnon and Molgaard 1991). If this is the case, what was previously interpreted as pristine, undeformed ice at the ice-indentor interface after unloading (so-called 'blue zones') may have been strongly deformed - or structurally 'damaged' - ice. Highly recrystallized ice is translucent, and no evidence of its deformation would be noticeable from video monitoring.

Another issue that could benefit from further investigation is the effect of loading on the temperature of the ice. A rise in temperature is expected upon the application of high axial stress. This rise corresponds to a release in thermal energy as a response to loading, with the possible contribution of frictional heating as the ice deforms. At high hydrostatic levels, which decrease the melting point of ice, this temperature rise may be sufficient to bring the ice, at least locally, to its melting point. The latent heat of fusion absorbed from the surrounding ice as a result of melting should contribute to a decrease in temperature.

2. Purpose and Methodology

The main objectives of the research presented in this report are three-fold:

- To investigate the effect of hydrostatic pressure on the deformational behaviour of ice specimens produced in the laboratory.
- To investigate the effect of temperature on the deformational behaviour of these specimens and provide an estimate of the activation energy for the deformation at various confinement levels.
- To establish a comparative basis between the deformational behaviour of laboratory-produced ice and naturally formed ice of glacial origin.

Other themes of interest include:

- The effect of loading on the thermal behaviour of the ice.
- The behaviour of the ice up to very large strains and damage analysis.

Research on these other themes is on going as of this writing and will be reported elsewhere.

We begin with a section describing some of the basic notions related with triaxial deformation, the rheology of ice and the concept of 'temperature'. This is an attempt to make the text somewhat self-explanatory in terms of the approach, terminology and background relevant to the later sections. A review of the existing literature on the triaxial testing of ice is then provided. This is followed by a description of the experimental procedures, the results and a discussion. Appendix 1 encloses a detailed account of previous investigations. Appendix 2 provides photographs of various features related with the test specimens and their internal structure. The data is in Appendix 3.

3. General Notions and Principles

3.1. Stress

Stress is a force normalized over an area. It is a second-order tensor, which means that it has two free indices: its magnitude depends on both the orientation of the force and that of the surface on which it acts. This is usually represented as follows:

$$\sigma_{ij} = \begin{bmatrix} \sigma_{11} & \sigma_{12} & \sigma_{13} \\ \sigma_{12} & \sigma_{22} & \sigma_{23} \\ \sigma_{13} & \sigma_{23} & \sigma_{33} \end{bmatrix} \qquad \textit{Eq. 1}$$

The stress conditions that are simulated with ice specimens in the laboratory are those corresponding to the equation below (whereby $\sigma_{ij} = 0$) because they are simpler to obtain: only the three principal stresses (σ_{11}, σ_{22} and σ_{33}) need to be controlled.

$$\sigma_{ij} = \begin{bmatrix} \sigma_{11} & 0 & 0 \\ 0 & \sigma_{22} & 0 \\ 0 & 0 & \sigma_{33} \end{bmatrix} \qquad \textit{Eq. 2}$$

It is also more representative of the stress acting on a free body element when one of its reference axes is parallel to the direction in which the load is applied onto the ice (this point is illustrated in Figure 2 for a two-dimensional case).

A uniaxial stress is one in which one principal stress, either σ_1 (for a compressive stress) or σ_3 (for a tensile stress), is non-zero and the other two are equal to zero. Uniaxial testing may be done, for instance, to study the mechanical behaviour of the ice near one of its free surfaces (location *A* in Figure 2). A biaxial stress is one in which two of the three principal stresses are nonzero and the third one is zero. A triaxial state of stress is one in which all three principal stresses are non-zero. This will generally be the case in an ice

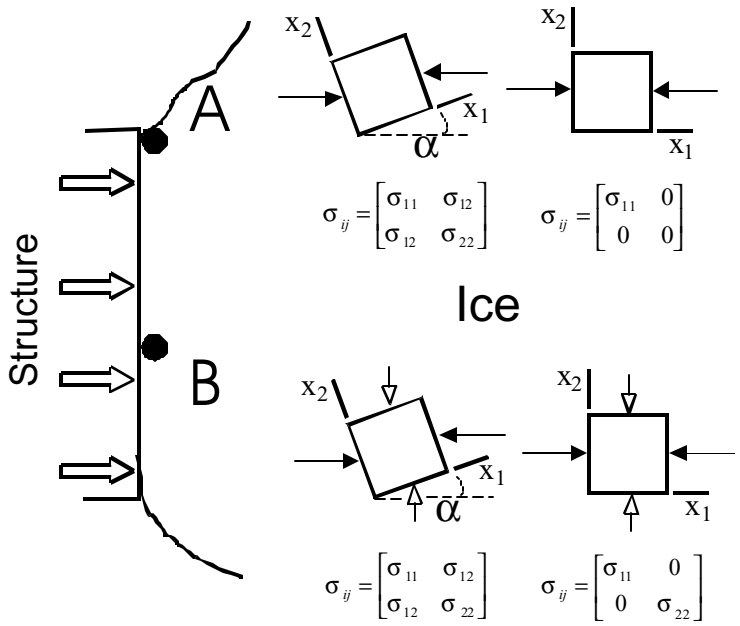

Figure 2: The stress at a point, represented by a free body element, and equivalent stress tensors for two different locations along the ice-structure interface. The reference axes to the left are at an angle α with the compression direction of the indentor, and $\sigma_{ij} \neq 0$. To the right, the references axes are chosen so that one axis is parallel to the compression direction, and $\sigma_{ij} = 0$. Near a free surface (location A), only the compressive forces from the indentor and their reaction (black arrowheads) will act on the ice. Away from the free surfaces (location B), the ice exerts a confinement (white arrowheads).

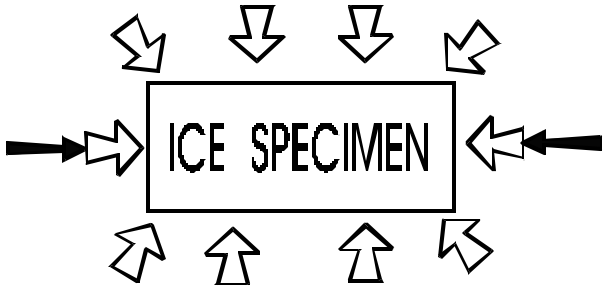

Figure 3: Loading regime on an ice specimen. The white and black arrows symbolize the confinement and axial compressive load, respectively.

body, except at locations very near the free surfaces. The reason for this is that, elsewhere, the ice exerts a given level of confinement during the deformation, which will increase with distance away from the free surfaces (location *B* in Figure 2).

The stresses to which ice may be submitted and the deformation that results from it are divided into two fundamentally distinct states. The first one involves a change in volume, whereby the crystal lattice remains intact but the constituents' atoms and molecules are forced either closer together (contraction) or farther apart (dilation). The stress causing this condition is referred to as *hydrostatic* (or *isotropic*) and leads to a deformation that is elastically recoverable. The second state involves a distortion in the crystal lattice and ultimately leads to a permanent change in shape due to the break up of atomic bonds. This is known as a *deviatoric* stress. It is the deviatoric component that causes the material to fail or yield, either in a brittle fashion, through the formation and propagation of cracks, or in a ductile fashion, through recrystallization and other processes.

The total stress is the summation of the hydrostatic and deviatoric components:

$$\begin{bmatrix} \sigma_{11} & \sigma_{12} & \sigma_{13} \\ \sigma_{12} & \sigma_{22} & \sigma_{23} \\ \sigma_{13} & \sigma_{23} & \sigma_{33} \end{bmatrix} = \begin{bmatrix} p & 0 & 0 \\ 0 & p & 0 \\ 0 & 0 & p \end{bmatrix} + \begin{bmatrix} (\sigma_{11} - p) & \sigma_{12} & \sigma_{13} \\ \sigma_{12} & (\sigma_{22} - p) & \sigma_{23} \\ \sigma_{13} & \sigma_{23} & (\sigma_{33} - p) \end{bmatrix} \qquad \textit{Eq. 3}$$

where p is the hydrostatic pressure, also called *mean stress*, and given by:

$$p = \frac{(\sigma_{11} + \sigma_{22} + \sigma_{33})}{3} \qquad \textit{Eq. 4}$$

This equation is a generalized form for the stress conditions that may exist at a given location inside the ice body. As mentioned earlier, we are able to simplify this situation by considering an equivalent set of stress conditions with the three mutually perpendicular planes along which all σ_{ij} stresses are zero. Thus,

$$\begin{bmatrix} \sigma_{11} & 0 & 0 \\ 0 & \sigma_{22} & 0 \\ 0 & 0 & \sigma_{33} \end{bmatrix} = \begin{bmatrix} p & 0 & 0 \\ 0 & p & 0 \\ 0 & 0 & p \end{bmatrix} + \begin{bmatrix} (\sigma_{11} - p) & 0 & 0 \\ 0 & (\sigma_{22} - p) & 0 \\ 0 & 0 & (\sigma_{33} - p) \end{bmatrix} \qquad \textit{Eq. 5}$$

This represents the stress existing inside the ice body when one of the reference axes (σ_{11}) is parallel to the direction of relative motion between the ice and the indentor.

It is possible to obtain a basic reproduction of this stress regime by conducting triaxial tests, involving the superposition of a confinement and a uniaxial stress. The equipment we used for our investigations allows us an independent control over these two stresses. The first one is obtained by compressing the oil in which the ice specimen is immersed. The second one is obtained by loading the specimen axially. This is shown schematically

in Figure 3. For example, if we were to submit an ice specimen to a 50 MPa confinement (white arrows) and a 15 MPa axial compression (black arrows), the stress along the compressive axis (σ_1) would be equal to the summation of both stresses - corresponding to 65 MPa. The stresses along the other two axes (σ_2 and σ_3) would both be 50 MPa. The hydrostatic stress is then 55 MPa. The deviatoric stresses are as 10, -5 and -5 MPa, respectively, for σ_1, σ_2 and σ_3.

3.2. Strain

Strain is a measure of deformation. In a specimen, it is expressed as a difference between the original (L_0) and deformed (L) length of a material line (which, for small increments, may be represented by dL). The *engineering strain* is the deformation normalized over the original length:

$$\varepsilon_E = \frac{(L_0 - L)}{L_0} \quad \text{or} \quad d\varepsilon_E = \frac{dL}{L_0} \qquad \textit{Eq. 6}$$

The total, or *true*, strain can be obtained by integration:

$$\varepsilon_T(t) = \int_{L_0}^{L_t} \frac{dL}{L_0} = \ln \frac{L(t)}{L_0} = \ln\left[1 - \frac{(L_0 - L)}{L_0}\right] = \ln\left[1 - \varepsilon_E\right] \qquad \textit{Eq. 7}$$

With increasing deformation, the true strain becomes progressively larger than the engineering strain. The use of the true strain is more appropriate when deformation exceeds a few percent.

Strain is also a second-order tensor. The strain tensor can be resolved into an isotropic and a deviatoric component:

$$\begin{bmatrix} \varepsilon_{11} & \varepsilon_{12} & \varepsilon_{13} \\ \varepsilon_{12} & \varepsilon_{22} & \varepsilon_{23} \\ \varepsilon_{13} & \varepsilon_{23} & \varepsilon_{33} \end{bmatrix} = \begin{bmatrix} \varepsilon_H & 0 & 0 \\ 0 & \varepsilon_H & 0 \\ 0 & 0 & \varepsilon_H \end{bmatrix} + \begin{bmatrix} (\varepsilon_{11} - \varepsilon_H) & \varepsilon_{12} & \varepsilon_{13} \\ \varepsilon_{12} & (\varepsilon_{22} - \varepsilon_H) & \varepsilon_{23} \\ \varepsilon_{13} & \varepsilon_{23} & (\varepsilon_{33} - \varepsilon_H) \end{bmatrix} \qquad \textit{Eq. 8}$$

where ε_H is the isotropic strain:

$$\varepsilon_H = \frac{(\varepsilon_{11} + \varepsilon_{22} + \varepsilon_{33})}{3} \qquad \textit{Eq. 9}$$

3.3. Type of Tests

Two loading regimes are most commonly used in ice engineering.

3.3.1. Creep test

The word *creep* is often used to describe time-dependant deformation under any loading regime. A more rigorous definition is when a constant stress is applied to a specimen, which then undergoes a progressive deformation with time (*e.g.* Popov 1990). In most cases, the area through which the load is transmitted either increases (in compression) or decreases (tension) as the specimen deforms, so that the stress is only nominally constant under constant load. Because time-dependant deformation mechanisms (related with the motion of crystal defects) are thermally-activated, creep tests can only be done at a temperature that is close to the melting point of the material, as is the case for most ice engineering applications. Creep will occur at lower temperatures but at a time scale that is too long to be practical for testing and that may not be relevant to engineering.

3.3.2. Constant Strain-Rate Test

In this case, the force applied onto the specimen varies to maintain a constant strain-rate. This test is often referred to as a *strength test*, because it records the stress at which the material yields. The relative displacement of the platens is hydraulically-controlled by a closed-loop feedback from displacement gages that are attached directly onto the specimen. This allows the compliance of the testing system to be excluded from the measurements (Sinha 1979a, 1981a,b). With this method, only the deformation at the centre of the specimen is considered, leaving out that occurring near the platens, which is non uniform due to the boundary conditions. Constant strain rate tests are usually more popular in the ice engineering community because they provide numbers on the strength of ice and its strain-rate sensitivity.

3.3.3. This study

Only creep testing was done as part of this study. The reason was that our investigations were originally designed to be an extension of an earlier testing program in which specimens were submitted to a constant load (Meglis et al. 1999, Melanson et al. 1999a). Another reason is the technical challenge related with the use of displacement gages attached onto the ice specimens: the latter were enclosed in a latex jacket to prevent penetration of the confinement fluid during deformation. Also, large strains were achieved in our tests, leading to a substantial change in specimen morphology and the resulting difficulty in maintaining the gages in position. The strain in the specimen could therefore only be measured by monitoring the displacement between the platens.

A correspondence between constant strain rate and constant load tests was established by Mellor and Cole (1982, 1983) and Sinha et al. (1995). They have shown that, when properly interpreted, creep curves can also provide information on the failure strength. The ultimate yield strength in this type of tests is the equivalent to the minimum strain rate for a material submitted to a constant stress. This means that if a constant strain rate test, done with a strain rate X, results in a strength Y, the same material submitted to a constant stress Y should display a minimum strain rate of X (Figure 4).

The minimum strain rate is a useful index: it allows to monitor the relative ‘compliance’ of the material under different loading conditions. The higher the minimum strain rate the

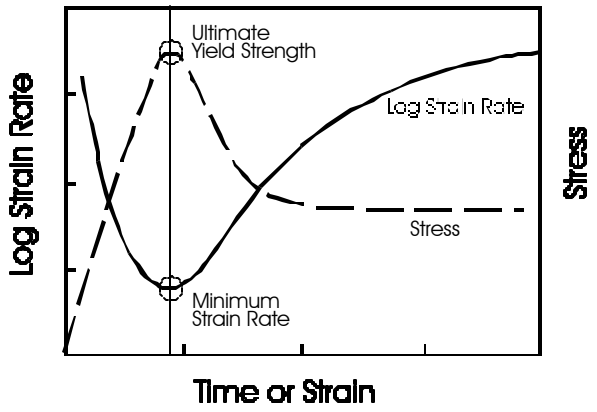

Figure 4: Response of ice when it is submitted to 1) a constant stress (for which the strain rate is recorded) and 2) a constant strain rate (for which the stress is recorded). The minimum strain rate in the former is equivalent to the ultimate strength in the latter.

more compliant is the ice. On the basis of the aforementioned correspondence, we would expect the ultimate yield strength of the ice to decrease with the same change in loading conditions.

3.4. Constitutive modeling

The rheological behaviour of a material is specified by the relationship between dynamic (stress) and kinematic (strain) quantities. C*onstitutive modeling* is a mathematical expression of this behaviour. The relationship also involves intrinsic (material properties such as mass, elastic properties, viscosity,...) and extrinsic (time, temperature, pressure, ...) parameters. Newton's Second law of Motion $F=ma$ is an example, relating a dynamic (force F) and a kinematic (acceleration a) quantity, with an intrinsic material parameter (mass m). A more general form of this relationship may be

$$D = f(K, I_p, E_p) \qquad \textit{Eq. 10}$$

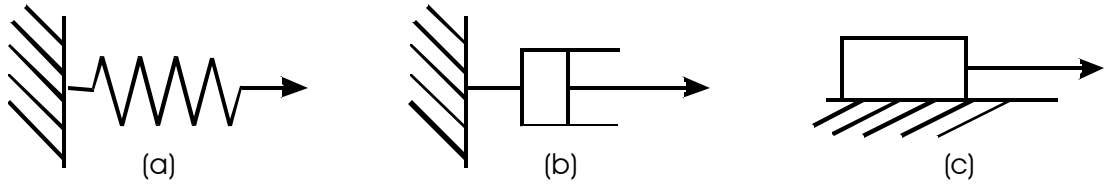

Figure 5: A few elements used to visualize the mechanical response of a material. a) Spring, b) dashpot, c) block maintained in place by friction.

where D represents the dynamic quantity (force, stress, stress rate, ...), K represents the kinematic quantities (displacement, velocity, strain, strain rate,...), and I_p and E_p are the intrinsic and extrinsic parameters, respectively.

One of the main purposes of experimental work is to provide information on the nature of that relationship.

A classification scheme has been devised in continuum mechanics to represent a number of rheological behaviours. This scheme uses conceptual elements, including a spring, a dashpot and a body resting on a surface and maintained in place by friction (Figure 5).

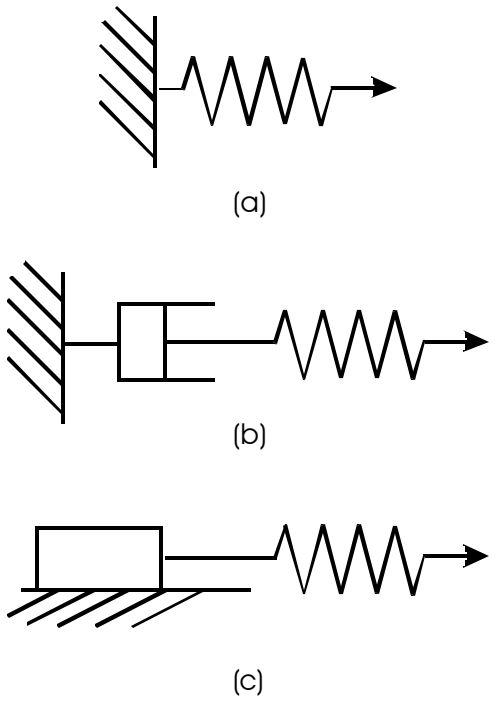

Figure 6: Three common type of rheological behaviours. a) Elastic, b) visco-elastic, c) plastic.

These are combined in a variety of ways to generate a stress-strain behaviour, also known as *phenomenological* behaviour, that compare with the actual response of the material to given loading conditions. The spring on its own reproduces the *elastic* response; a combination of a spring and a dashpot represents *visco-elasticity*; and a combination of a spring and a body in frictional contact with the surface corresponds to *plasticity* (Figure 6).

3.4.1. Elasticity

Elasticity is a phenomenon that can be linked directly with the structural nature of the material: it is the macroscopic expression of the electro-magnetic forces that keep individual atoms at an 'equilibrium' distance from each other. This is the reason why

elastic deformation is reversible. The magnitude of these forces depend on the length of the bond, and how it is defined: in general, covalent bonds are stronger than metallic bonds, which are in turn stronger than ionic bonds. Temperature affects the length of the bonds and this will be discussed later. Most materials behave elastically under small

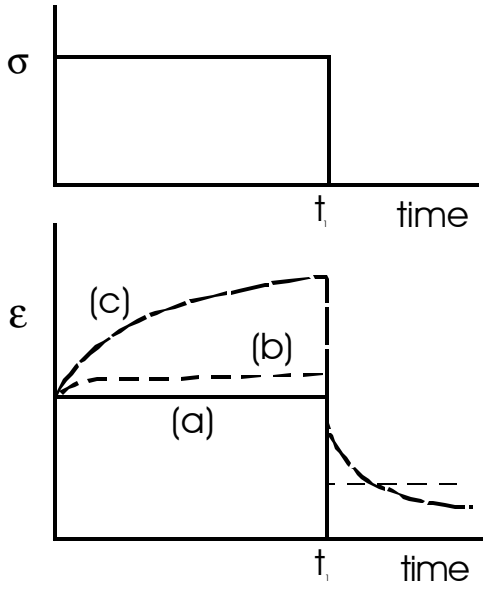

Figure 7: Rheological behaviours on a strain-time diagram, upon the application of a stress. a) elastic, b) visco-elastic, c) plastic.

loads. Both the deformation and recovery are time-independent (Figure 7). The stress-strain behaviour is linear and is described by Hooke's law ($\sigma = E\varepsilon$ shown in Figure 8a). This relationship is usually applied to a change in length. The material constant *E*, also called Young's modulus, may be replaced by a shear modulus to describe the elasticity of shape, or by a bulk modulus to describe the volume elasticity.

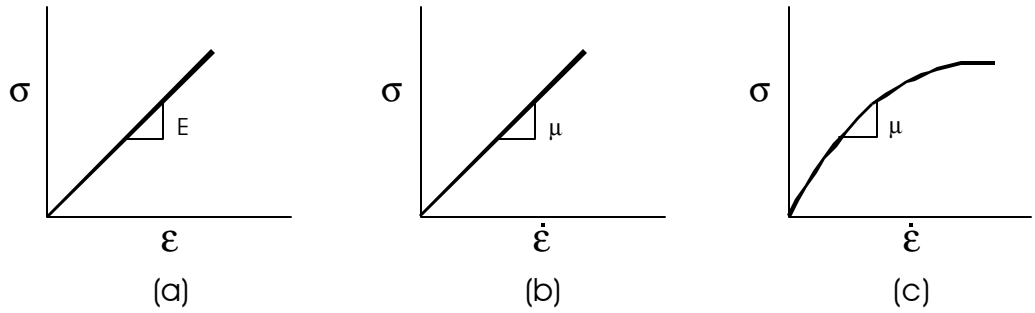

Figure 8: Rheological behaviour corresponding to a) elasticity, b) linear visco-elasticity and c) non linear visco-elasticity. Note that that stress is plotted against strain rate in (b) and (c).

3.4.2. Visco-Elasticity

Once the elastic limit is reached, visco-elastic materials display a gradual increase in strain but at a decreasing strain rate. Stress removal at time t_1 leads to the instantaneous elastic recovery, followed by a time-dependant or 'delayed' elastic component (Figure 9). In terms of the mechanical response to loading, ice is best described as a visco-elastic material. The establishment of a physical basis for visco-elasticity is more complex than in the case of elasticity. They are tied in not only with the bonding energy but also with generation and motion of crystal defects (dislocations, vacancies, diffusion-related phenomena, ...) and, depending on the external parameters such as pressure and temperature, the formation of microcracks. Mechanisms accounting for this type of behaviour must also involve grain boundaries. Indeed, the deformation of single ice crystals has been shown to differ significantly from polycrystalline ice. Firstly, the elastic response is followed by accelerating instead of decelerating creep[1]. Secondly, the creep of single crystals does not display a delayed elastic component.

Viscosity may be expressed as

$$\dot{\varepsilon} = \frac{\sigma^n}{\mu} \qquad \textit{Eq. 11}$$

where $\dot{\varepsilon}$ is the strain rate, σ is the stress and μ is the viscosity. For linear visco-elastic solids (also known as *Newtonian*), n =1 and the material behaves like a liquid[2]. For non-linear visco-elastic solids, $n > 1$.

3.4.3. Plasticity

Plasticity often designates the deformation occurring after the elastic limit is reached (that is, when the force applied to the material is high enough to overcome the strength of the atomic bonds). The word *anelasticity* is also used as for that purpose. The ice response to loading is thus commonly referred to as plastic in the engineering literature. A more rigorous usage of the term plasticity implies a particular behaviour of the strain once the elastic limit is exceeded: the strain increases a little more before stabilizing to a constant

---

[1] Accelerating and decelerating creep are discussed later.

[2] The notion that a solid substance may flow like a liquid may be better understood by considering the *Deborah number D.* This is the ratio of the time required for a measurable amount of creep over the time during which the observation is done and limited to the life expectancy of the observer. If D is small, we perceive the material as a liquid. If D is large, it is seen as a solid. In both cases, there is linear relationship between $\dot{\varepsilon}$ and σ (which is characteristic of what we acknowledge as a liquid on an every day basis).

value. The elastic deformation is recovered upon the removal of the stress, and a permanent strain remains, without a delayed elastic component. Plasticity does not describe the phenomenological response of ice. The concept of visco-elasticity is preferred for this purpose.

3.5. The Rheology of Ice

3.5.1. Phenomenology

Figure 9 is a typical creep response of polycrystalline ice observed during our investigations. This behaviour is often represented conceptually by Figure 10. The delayed elasticity is simulated by a combination of a dashpot and a spring arranged in parallel, referred to as a *Kelvin* unit. The combination of a dashpot (viscous strain) and a spring (elastic strain) arranged in series is known as a *Maxwell* unit. The entire assembly is called a *Burgers'* model and is the one that is most commonly used to express the creep of ice. The total strain ε_T is therefore

$$\varepsilon_T = \varepsilon_E + \varepsilon_D + \varepsilon_P \qquad \textit{Eq. 12}$$

The elastic deformation ε_E in a standard creep test is a very small portion of the total deformation (typically 0.1 to 0.5% strain, depending on loading rate). It is therefore not a significant issue in this study, particularly if we focus on very high strains. The delayed elastic deformation ε_D has been attributed to grain boundary sliding (Sinha 1979b, 1984a). This phenomenon takes place immediately after the elastic strain and is also a relatively small part of the total deformation. It induces a decelerating phase in the early part of the deformation (*A* in Figure 9). The permanent strain ε_P is the deformation that results from the generation of microcracks and/or the motion of crystal defects. These mechanisms begin as soon as the load is applied but their contribution to the total deformation is initially negligible. It becomes more important as the deformation rate reaches a minimum (*B*) and begins to accelerate (*C*).

The terms 'primary', 'secondary' and 'tertiary' creep is used consistently in the ice literature to designate stages A, B and C in Figure 9. This usage has an historical basis: it was borrowed from metallurgical studies, in which metals and alloys undergoing creep spend most of their design life span in the secondary stage. This is not the case for ice, where the secondary creep is no more than an inflexion point between a decelerating and an accelerating phase. This terminology is therefore not retained in the present report.

3.6. Temperature

3.6.1. Basic Concept

Physically, temperature is the amount of kinetic energy, or *heat*, stored by the individual atoms making up a given substance (gas, liquid or solid). This energy corresponds to a large extent to the vibration of the atoms about their equilibrium position. The melting

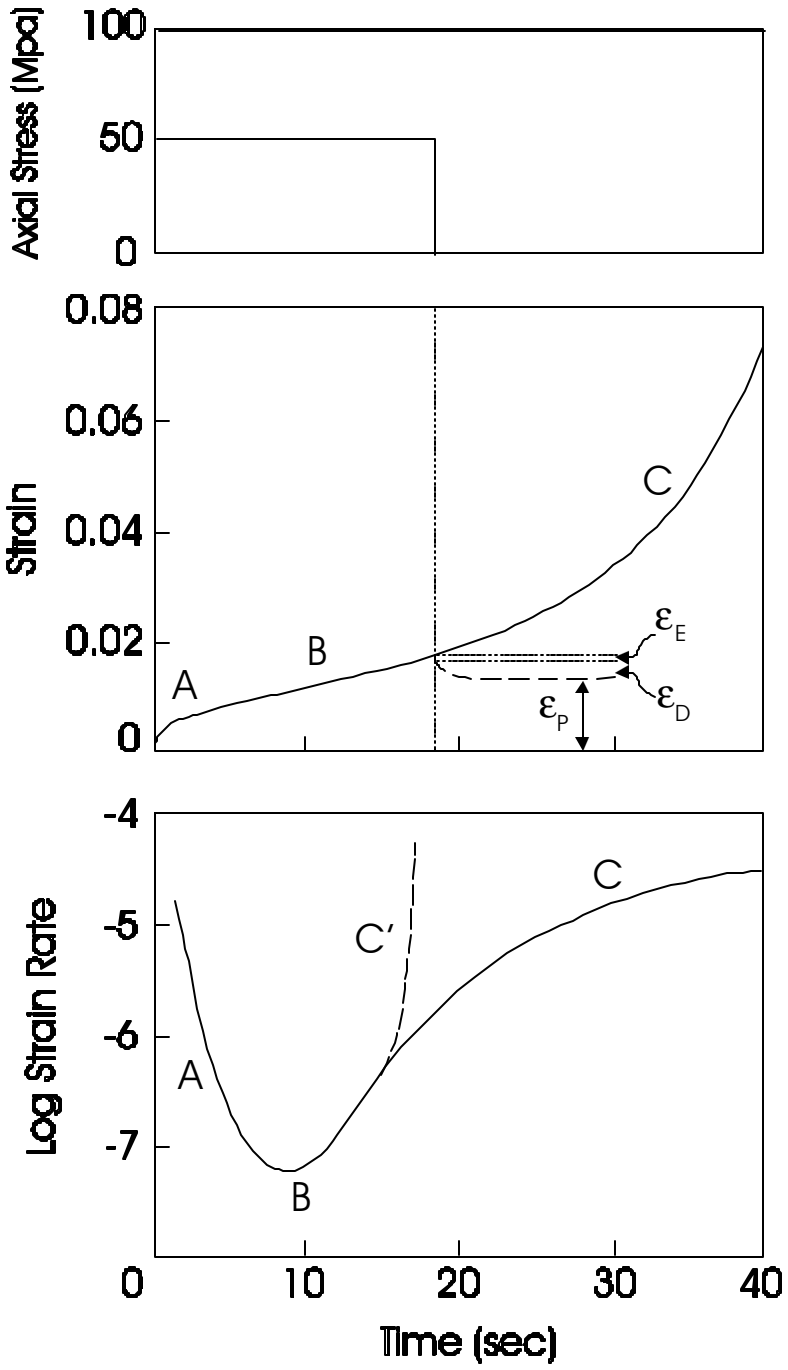

Figure 9: Creep response for freshwater, polycrystalline ice at 55 MPa hydrostatic pressure, 15 MPa axial stress and a temperature of -10°C. The elastic (ε_E), delayed elastic(ε_D) and permanent (ε_P) component of the deformation are best seen upon unloading the specimen. A: Decelerating creep, B: Minimum creep rate, C: Accelerating creep, C': Run-away behaviour.

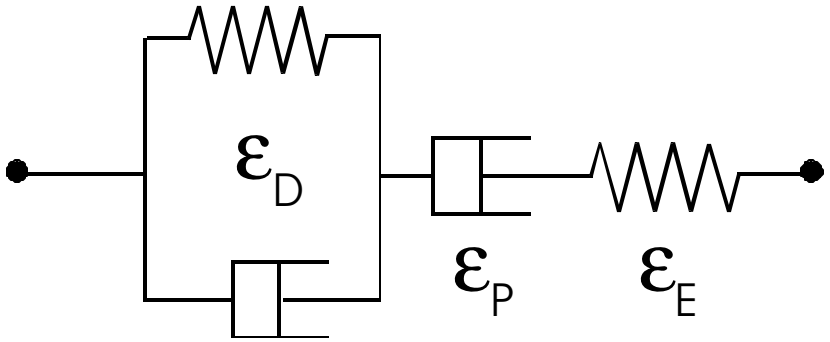

Figure 10: Behaviour of polycrystalline ice, shown by a combination of springs and dash-pots.

point of a crystalline substance is reached when the amplitude of the vibrations is such that it is able to overcome the molecular bonding energy. Substance with weaker bonds will have a lower melting point. *Absolute zero* on the Kelvin temperature scale (-273°C) is a theoretical value at which atomic vibrations in all substances cease to exist. At that temperature, matter becomes inert and one may envisage air molecules lying on the ground, no longer able to surmount gravitational attraction.

A consequence of the Second Law of Thermodynamics is that energy spontaneously tends to flow only from where it is concentrated to where it is diffused. Consequently, it spreads out. In some cases, such as the cooling down of a frying pan when it is taken off the kitchen stove, this phenomenon will take place instantaneously. But there are other cases where it will not because of the existence of molecular bonding. This applies, for instance, to any form of fuels. Wood or coal will react with oxygen to form CO_2 and H_2O, which have a lower energy configuration. The difference in energy is dissipated in the form of 'heat'. But this reaction will only occur if the energy barrier, called *activation energy* and represented by molecular bonding in the reactants, is overcome. (This can be done quite effectively, in the case of a liquid fuel, with a lighted match.) The determination of the activation energy will be addressed in this report as it is a useful indication of what mechanism controls the deformation of the material.

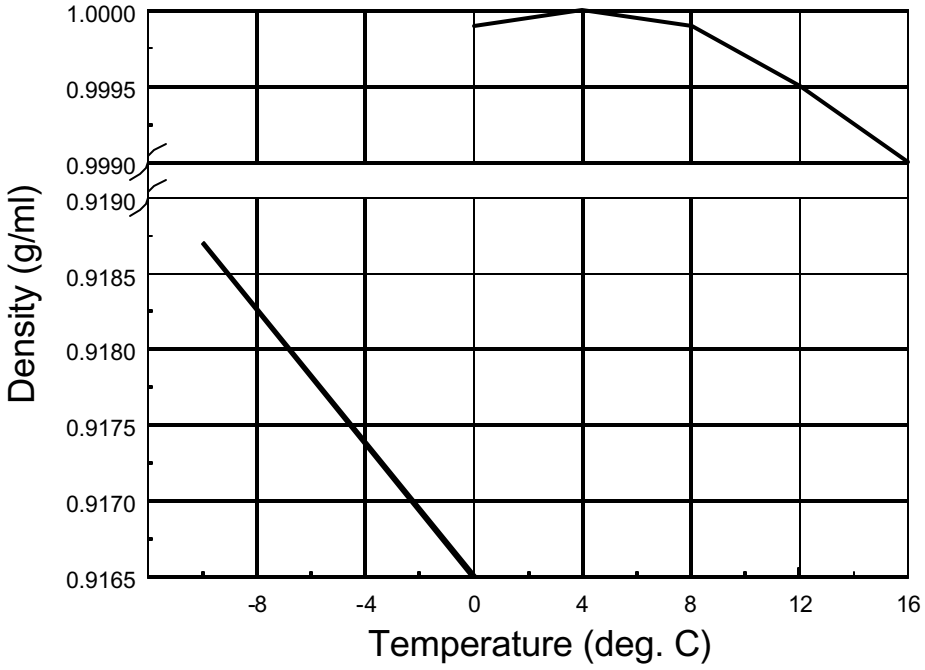

Figure 11: Density variation of ice and water across the phase transition. The data is from Bolz and Tuve (1970) and Hobbs (1974).

3.6.2. Physics of ice behaviour near its melting point

The oxygen atom in a H_2O molecule is more electronegative than the hydrogen atom, and the resulting H-O bonds have a 39% ionic character (Metcalfe et al. 1974). Consequently, the electrons are on average concentrated around the oxygen nucleus. Since the covalent bonds of the water molecule do not line up (the angle between the two bonds is about 105^o), it has a polar character. This polarity causes water molecules to be attracted to each other, thus defining the weaker *hydrogen bond*. In the solid phase (ice), H_2O molecules are arranged in a hexagonal crystal structure.

Above absolute zero (0^oK), the atoms making up the ice structure (or any other crystalline substances) vibrate. They do so anharmonically (out of phase), so that an increase in temperature induces an increase in volume, and a consequent reduction in density (Figure 11). As temperature increases, the bonds are stretched further and begin to break, the macroscopic expression of which is referred to as *melting*. Since the hexagonal crystal structure of ice is known to be very open, the water molecules can easily fit inside this structure once the bonds are broken. Doing so, they take up less space than when they were part of the crystal structure, which accounts for the increase in density across the phase change (Figure 11). The density then increases again slightly in

the liquid phase to a maximum of 1.0000 g/ml at 4°C, before dropping again. This is explained by the occurrence of two competing phenomena: 1) The on-going breaking down of the hydrogen bonds allows the water molecules to get closer together; 2) The increase in thermal energy overcomes the polar attraction between water molecules (Metcalfe et al. 1974). The first mechanism predominates only up to 4°C.

According to the Clapeyron equation,

$$dT_m = \frac{T_m (v_w - v_i)}{L_f} dp = -A dp \qquad \textit{Eq. 13}$$

where T_m is the melting temperature of ice in degrees Kelvin, p is pressure, L_f is the latent heat of melting per unit mass and v_i and v_w are the specific volume of ice and water, respectively. For ice, A = 0.0743°C / MPa at 0°C and 0.0833 °C / MPa at -10°C. At a pressure of 70 MPa, the ice specimen would be expected to melt at about 5.5°C. At a temperature of -10°C, melting occurs at 120 MPa. This is a direct consequence of the fact that ice expands upon freezing. A close examination of the following equation, derived from the one above, will help better understand this phenomenon:

$$\frac{dT_m}{dp} = \frac{(v_w - v_i)}{(e_w - e_i)} \qquad \textit{Eq. 14}$$

where e_w and e_i are the entropy of water and ice, respectively. The denominator of the right-hand term will necessarily be positive since entropy, which is the amount of disorder, is always higher in the liquid than it is in the solid. In the hypothetical case where the change of phase would *not* be accompanied by a change in volume, the melting point would not be affected by pressure (A = 0). Other materials that contract upon melting include Pu, Ge, Si, Bi, Sb and Ga (Poirier 1985). For most materials, however, the solid to liquid transition causes an increase in volume. If this phase change occurs when the material is at a high pressure, more energy will be required to compensate for the additional work exerted on the system by that pressure. This means melting will take place at a higher temperature. The *opposite* holds for ice since it looses volume upon melting (Figure 11).

Another outstanding feature with ice is its comparatively high degree of brittleness even when it is near or at its melting point. Most other crystalline substances will behave like soft putty near their melting temperature. The reasons for this unusual behaviour is tied in with a very low dislocation mobility and a high stability of its lattice structure, the latter resulting in a low solid solubility of vacancies and impurities (Barnes et al. 1971).

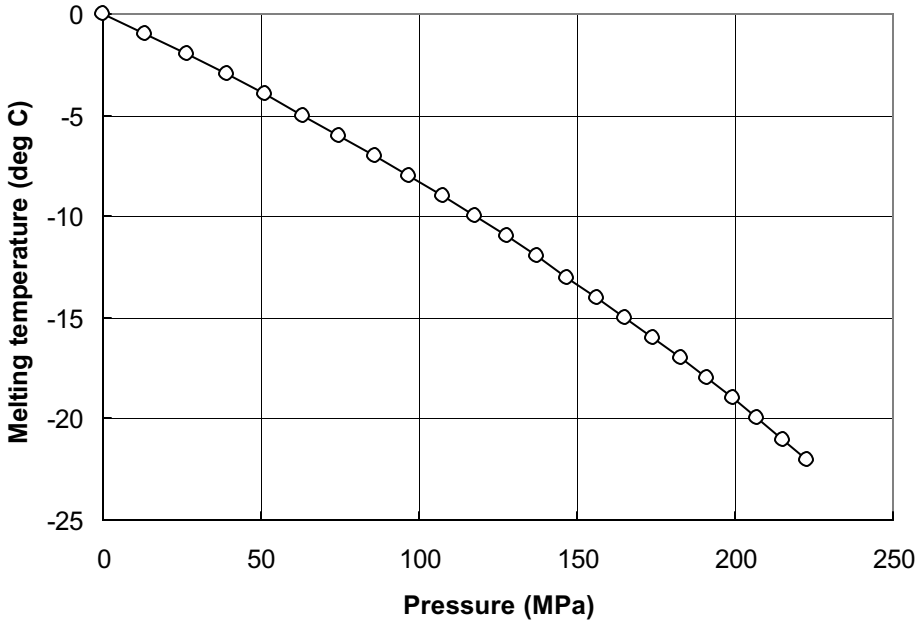

Figure 12: Variation of the melting temperature of ice with pressure (Nordell 1990).

3.6.3. Temperature considerations in triaxial testing

For the purpose of the following discussion, the *system* refers to what is enclosed in the triaxial cell (the ice specimen and the confining oil). According to the First Law of Thermodynamics, the change in the internal energy of this system (ΔU) is equal to the thermal energy Q transferred to the system minus the work W done by the system on its surroundings:

$$\Delta U = Q - W \qquad \textit{Eq. 15}$$

Q is negative when the thermal energy is transferred *from* the system. Similarly, W is negative if the work is done *on* the system. In the case of ice specimens, the internal energy is represented mostly by the thermal energy (the kinetic energy of the atoms) and the strain energy (the elastic energy stored in the crystal lattice). Other forms of internal energy, such as nuclear energy and chemical energy, can here be neglected. If we assume that the system is thermally isolated, or *adiabatic*, then there is no heat transfer in or out of the system ($Q = 0$). Thus $\Delta U = -W$. This situation roughly approximates our triaxial test conditions[1]. The work W is represented either by an increase in confinement and/or

[1] The triaxial cell we used is made out of steel so it is far from being thermally insulated. But heat transfer across the wall of the cell is relatively slow and is therefore neglected for the purpose of this discussion.

the application of an axial load. Either way, it is negative, leading to an increase in internal energy.

One question that is of interest concerns the amount of thermal energy absorbed by the ice during testing. Only 5 to 10% of the energy applied onto a any given specimen is stored in the defect structure (Nemat-Nasser 2000, p. 431). This implies a significant departure from isothermal conditions. If heat flow takes place (in the case the deformation is not entirely adiabatic), either by conduction through the end platens or the confining oil, this will lead to a non-uniform temperature distribution in the deforming specimen. This is an issue that has not attracted a lot of attention from the ice engineering community. Its relevance lies in the fact that the compressive strength of ice is a function of its temperature.

4. Previous work

A survey of the open literature reporting triaxial test data on various types of ice was carried out as part of our investigations. Fifty papers, published between 1958 and 2001 inclusively, were retrieved (Barrette 2001). This compilation only considers papers enclosing triaxial test data, and leaves out numerical and theoretical treatments. Testing under biaxial stress or plane strain conditions (*e.g.* Frederking 1977, Sinha 1984b, Timco and Frederking 1986) was therefore not included. Investigations on the elastic properties of ice under confinement were not searched either. The reader is referred to Gagnon et al. (1988) for this topic. Moreover, all of the data encountered were obtained from the hexagonal polymorph of ice (Ih) with few exceptions (*e.g.* Kirby et al. 1985, Durham et al. 1996). These were also omitted. Finally, only the English literature was surveyed.

The results of our search is presented in Appendix 1 (the abbreviations used in this appendix are explained in Table 1).

Both artificial and naturally-occurring ice types were investigated. The control on the deviator was generally done in two ways. Constant strain rate tests are those for which either specimen deformation or the rate of relative displacement between the upper and lower platen was kept constant. Constant stress - or creep - tests were also used. The stress was usually nominal since few investigators (*e.g.* Jones 1978, Mizuno 1992, Melanson et al. 1999a) reported a correction to compensate for a change in specimen area (required especially when large strains are achieved). All confined testing was done with a compressive axial stress, with the exception of Rigsby (1958)(shear) and Haynes (1973) (tension). In a few cases, a damage mechanics approach, instead of conventional visco-elasticity, was applied to the behaviour of ice to acknowledge the effect of load history on further incremental deformation (*e.g.* Jordaan and collaborators). Maximum axial stress is indicated for constant load tests; the logarithm of strain rate is indicated for constant

Table 1: List of abbreviations used in Appendix 1.

C	Columnar-grained
CR	Constant rate
CS	Constant stress
D	Damage
F	Freshwater (non-saline)
G	Granular (isotropic)
I	Iceberg
L	Laboratory-made
M	Monocrystalline
N	Naturally-occurring
P	Polycrystalline
S	Saline
1Y	First year sea ice
<1Y	Multiyear sea ice

strain rate tests. The temperature range of the test series is also indicated, along with the salient results.

Specimen confinement was usually delivered by a hydraulic fluid. In some cases, a constant ratio between axial and confinement stresses was maintained throughout the deformation. True multiaxial testing with brush-type platens, whereby loading along all axes of three-dimensional space is controlled independently, was also conducted. For these cases, no maximum confinement is shown in the results of our search. Discussions on the use of brush platens and multiaxial testing may be found in Haüsler (1981), Schulson et al. (1989), Haüsler et al. (1991) and Melton and Schulson (1998a). Following is a summary of these findings.

4.1. Effects of confining pressure

There is a general consensus that an increase in hydrostatic (or confinement) pressure causes an increase in the strength of freshwater (non saline) ice for constant strain rate experiments (Jones 1982, Mizuno 1998, Rist et al. 1988, 1994, Kalifa et al. 1989, 1992, Murrell et al. 1991, Nadreau et al. 1991) and a decrease in minimum strain rate for creep testing (Golubov et al. 1990, Jones and Chew 1983, Barrette and Jordaan 2001). This increase in 'compliance' has been observed at various creep loads and temperatures. It was also documented for natural or artificial sea ice (Nawar et al. 1983, Blair 1988, Cox and Richter-Menge 1988, Golubov et al. 1990, Sammonds et al. 1998, Rist. and Murrell 1994) and genuine iceberg ice (Nadreau and Michel 1986, Gagnon and Gammon 1995).

For strength tests, an increase in strain rate caused a steeper increase in the maximum deviator, following which the strength tend to level off.

A reversal in this trend was documented in studies that were able to investigate the deformational behaviour of ice at levels of hydrostatic or confinement pressures extending beyond 30 to 50 MPa. This was shown in constant strain rate tests, where the strength (or maximum deviator) reached a peak value between 10 and 50 MPa pressure (Durham et al. 1983, Kirby et al. 1985, Nadreau and Michel 1986, Richter-Menge 1991). A reversal was also documented with creep tests, whereby the minimum strain rate decreased with increasing pressure, then increased with further increase in pressure (Jones and Chew 1983, Barrette and Jordaan 2001). Furthermore, Jordaan and collaborators (see Jordaan et al. 1999, 2001) devised a formulation for the rate of damage in the accelerated zone of the creep curve. This rate was found to decrease up to hydrostatic pressure 30-40 MPa, and increase upon further pressure increase (Melanson et al. 1999a).

This reversal, or 'pressure softening effect', is generally attributed to the fact that, upon increasing pressure, the ice gets closer to its melting temperature. Locally, it may undergo melting, perhaps at specific locations along grain boundaries where stress cannot be readily accommodated by dislocation or diffusion-controlled deformation mechanisms. To the authors' knowledge no direct evidence of this phenomenon was presented to date. What may be stated is that an increase in pressure is thermodynamically equivalent to an increase in temperature. A better approach in the study of temperature effects may be to consider the temperature difference with respect to melting point, as opposed to the actual temperature at which testing takes place (Rigsby 1958).

4.2. Temperature and activation energy

An increase in temperature is known to cause a decrease in strength in constant strain rate experiments and an increase in strain rate for constant loading (Mellor and Testa 1969, Mellor 1980). This is also observed in specimens under triaxial pressure conditions (Durham et al. 1983, Cox and Richter-Menge 1988, Gagnon and Gammon 1995). This phenomenon is readily understood if one considers that a higher temperature induces an increase in the amount of kinetic energy within the material. Molecular bonding is therefore more easily overcome when submitted to additional energy in the form of mechanical stress.

The most commonly used formulation for the determination of activation energy follows the usual Arrhenius relationship:

$$\dot{\varepsilon}_{min} \propto \exp(\frac{-Q}{RT}) \qquad \textit{Eq. 16}$$

where σ is the axial stress, Q is the activation energy, R is the universal constant, T is the absolute temperature, A, n are constants. The parameter k (Boltzmann's constant) is also

used instead of R, depending on which units are used for energy. In some cases, Q is the activation enthalpy, and is defined as

$$Q = E + PV \qquad \textit{Eq. 17}$$

where E is the activation energy, P is the pressure and V is the activation volume (*e.g.* Jones and Chew 1983, Durham et al. 1983, Mizuno 1992).

Taking the natural logarithm on both side of the Arrhenius relationship,

$$\ln(\dot{\varepsilon}) = f(\frac{-Q}{RT}) \qquad \textit{Eq. 18}$$

Q can be determined from a plot relating the logarithm of strain rate and $1/T$. For creep tests, the minimum strain rate is considered for this exercise. For constant strain rate test, it is done with a formulation that combines the Arrhenius relationship and Glen's law:

$$\dot{\varepsilon}_{\min} = A\sigma^{n} \exp(\frac{-Q}{RT}) \qquad \textit{Eq. 19}$$

where σ is the yield strength of the ice, n is the stress exponent and A is a constant. We then have,

$$n\ln(\sigma) = \ln\dot{\varepsilon} - \ln A + \frac{Q}{RT} \qquad \textit{Eq. 20}$$

(see Kirby et al. 1985, for instance). A number of authors have reported an increase in activation energy towards the melting point of ice (see Table 3). This change in activation energy near melting point was observed only in polycrystalline ice, not single crystals, pointing out to role of grain boundaries (see Mellor and Testa 1969). Two mechanisms were invoked to explain this increase in activation energy: grain boundary sliding and the presence of liquid at triple junctions (Barnes et al. 1971).

Table 2: List of abbreviations used in Table 3.

AE	Activation energy
AT	Activation enthalpy
B	Bicrystals
C	Columnar-grained
CR	Constant rate
CS	Constant stress
D	Damage
F	Freshwater (non-saline)
G	Granular (isotropic)
I	Iceberg
L	Laboratory-made
M	Monocrystals
N	Naturally-occurring
P	Polycrystalline
P_c	Confining pressure
S	Saline
T	Temperature
1Y	First year sea ice
<1Y	Multiyear sea ice

Table 3: A selection of previous investigations on the activation energy of ice, arranged in chronological order by date of reference.

Investigator(s)	**Ice type**	**Test type**	**P_c (MPa)**	**Max. Dev. (MPa)**	**Log_{10} strain rate (s^{-1})**	**T (^oC)**	**Observations** Energies (AE, AT) given in kJ/mol
Mellor and Testa 1969	L,G,M, F	CS	0.1	1.18		-73 to 0	AE : 68.8 for T <-8°C, non linear relationship for T > -8°C
Barnes et al. 1971	L,G,F	CS	0.1			-45 to -2	AE : 79 for T <-8°C, 120 for T > -8°C
Gold 1973	L,C,F	CS	0.1	0.098		-40 to -5	AE: 15.5 kcal mol^{-1}
Homer and Glen 1978	L,G,M, B, F	CS	0.1	2		-20 to -4.5	AE: 78 for M; AE: 75 for B
Durham et al. 1983, Kirby et al. 1985	L,G,F	CR	up to 350		-6.5 to -2.5	-196 to -15	AT at 50 MPa P_c: 91 for -5 >T>-30, 61 for -30 >T>-78, 27 for -78 >T>-115C.
Mae and Azuma 1989	M,F / P,F		up to 56(ii)		-7	-20 to -5	Activation volume
Mizuno 1992	L,G,F	CS	5 and 35(ii)	3		-10 to -0.8	AT is 118 below -6°C at both pressures. At higher temperature, it increases to 207 and 240 for 5 and 35 MPa hydrostatic pressure respectively.
Rist and Murrell 1994	L,G,F	CR	up to 46	45	-5 to -2	-45 to -5	AE: 69
Gagnon and Gammon 1995	I	CR	up to 14		-4.3 to -1.3	-16 to -1	AE: 101

(i) Estimated. (ii) Hydrostatic (mean) stress. (iii) Multiaxial, brush-type platens.

5. Testing and Results

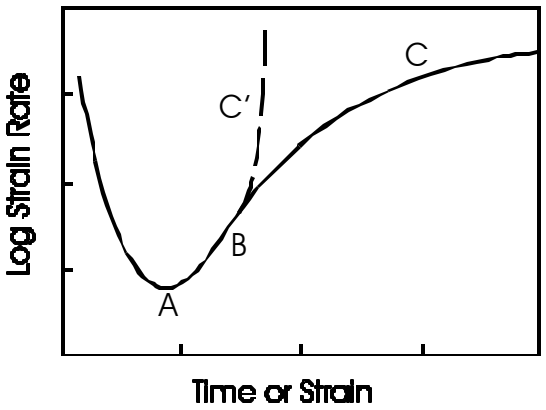

Figure 13: Point of interests in a typical creep curve.

5.1. Rationale

One of the main objectives of the experimental program carried out at Memorial University is to attempt to better define the ice response to loading for pressure and temperature conditions existing in a typical ice-structure interaction. We also address issues that have not yet been looked into. One is the pressure dependency of activation energy. Another, which will be reported elsewhere, is the behaviour of the ice up to large strains.

We consider a typical creep response for ice under a constant load, as shown in Figure 13. We are investigating three areas: 1) The *minimum creep rate* (A) is documented throughout the existing ice literature. This parameter is therefore used for correlation purposes with previous work. As mentioned already, it also provides information on the upper yield strength of ice (Mellor and Cole 1982, 1983, Sinha et al. 1995). 2) The *accelerating creep* (B) represents a nearly linear increase in strain rate following the minimum strain rate. This zone is currently interpreted to be representative of the deformation taking place at the ice-structure interface, where a layer of damaged ice was observed in medium-scale indentation field tests (Jordaan et al. 1999). A *damage* formulation has been applied to numerical simulations taking place in this layer. Data obtained in the course of this research is used to calibrate the model used for these simulations (Melanson et al. 1998). 3) The deformation rate at high strains either levels off (C) or indicate failure (C') of the ice specimen. Because of specimen distortion at this strain level, the interpretation of these data has to be done with care. This effort is worth while as it should lead to a better understanding of cyclic loading and extrusion processes taking place during the interaction (Jordaan et al. 1999, Jordaan 2001).

The present report focuses on the minimum strain rate (point A in Figure 13) and how it is affected by hydrostatic pressure up to 70 MPa and in a temperature range representative of that existing in nature.

5.2. Laboratory Procedures

A detailed description of the laboratory procedures is provided in PERD/CHC Report 75-13. An outline of these procedures is now presented. It includes slight variations that have been implemented since the above-mentioned report was written.

5.2.1. Production of ice specimens

Ice was grown in insulated buckets filled with distilled, de-ionized and de-aerated water from a single crystal platelet (or 'seed'). The resulting blocks consisted mostly of monocrystalline ice (no grain boundaries) that were cut with a band saw and crushed. The fragments obtained with this method were thus all single crystals, which were then sieved into two sizes. One between a mesh of 2 and 3.5 mm. The other was made from the fraction above 3.5 mm. Seeds from either size were put in a cylindrical mould and water was introduced into the mould under vacuum to fill in the voids between the seeds. The mould was then allowed to freeze completely leading to granular, bubble-free. In some unsuccessful cases, air entrapment occurred and this ice was also kept for testing.

The cylindrical mould was then cut into four quarters and machined into cylindrical specimens with a nominal diameter of 70 mm and a nominal length of 155 mm. These were stored at a temperature of -25°C for a time interval usually not exceeding a few weeks before testing.

The iceberg ice was purchased from a local iceberg harvester, who quarried it from a iceberg that was grounded near the north-eastern coast of Newfoundland in the summer of 2000.

5.2.2. Density and grain size

The density of 49 ice specimens is indicated in Table 4. The weight was obtained with a high-precision scale and the volume was derived from the dimension of the specimens after machining. The grain size of the laboratory-made ice was determined from the examination of several thin sections. The longest dimension of the ten largest grains in a given section was averaged, giving values of 9.8 and 10 mm, respectively, for the ice grown from normal and coarse grain seeds. The average grain area was also obtained from these sections, with values of 12.3 and 16.6 mm^2, respectively, for the ice made from normal and coarse seeds. The grain size of the iceberg ice has not been looked at in detail. In general, it varied somewhat and was significantly larger than the laboratory ice.

Table 4: Density of ice specimens, in g/ml (accuracy: 0.002 g/ml).

Ice Type	# of specimens	Aver. density	S.D.
Normal	11	0.912	0.002
Coarse	11	0.913	0.002
Bubbly	10	0.909	0.004
Iceberg	17	0.895	0.011

Additional information on grain size and shape for both laboratory and iceberg ice is available in Appendix 2.

5.2.3. Testing

Testing in compression under a confining load was conducted in the thermal laboratory of the Engineering Faculty at Memorial University. The parameters recorded included platen displacement, axial load, confining pressure and temperature. A Materials Testing Systems (MTS) test frame was fitted with a Structural Behaviour Engineering Laboratories Model 10 Triaxial Cell. The MTS system consisted of two servo-controlled hydraulic rams that applied axial load and confining pressure independently. The rams were controlled using MTS Test Star II software, operated on a 486 microprocessor-based computer with an OS/2 platform. The computer and software also performed data acquisition for each test.

A specimen was mounted on hardened steel end platens of the same diameter as the specimen and the assembly was then enclosed in a latex jacket to keep the confining medium (silicone oil) from penetrating the ice. The specimen assembly was then placed inside the triaxial cell, which was then closed and filled with silicone oil. The cold room was set to a target temperature, which was monitored using RTD sensors located within the confining vessel. The pressure was therefore raised in steps to the target level, so that adiabatic heating of the oil due to pressurization would not increase by more than 2°C. Inclusion of temperature probes *within* the specimen showed that the ice needed an additional two hours, once the target pressure was achieved, to equilibrate to the temperature of the oil.

The specified creep load, ranging between 56 and 59KN (depending on specimen diameter), was applied within 0.1 second. It remained at that level until the axial deformation reached 35 to 44% true strain. In some cases, specimens failed without yielding any creep data. This usually occurred with specimens machined from iceberg ice. At the end of each test the axial load was quickly removed and the confining pressure was released gradually. The specimen was removed from the cell immediately after testing.

5.3. Results

5.3.1. Overview of testing

Testing took place over a period of two years (between August 1999 and June 2001). A total of 55 successful tests have been done: 37 with laboratory-produced ice and 18 with iceberg ice. Hydrostatic pressures ranged from 10 to 70 MPa. Temperatures ranged between -26 to -6°C. Deviatoric (axial) stress was set at 15 MPa at the beginning of all tests but decreased substantially upon increase in surface area at large strains. No other deviatoric stresses were used, which allowed us to focus on the effects of pressure and temperature while limiting the scope of the research to a manageable size.

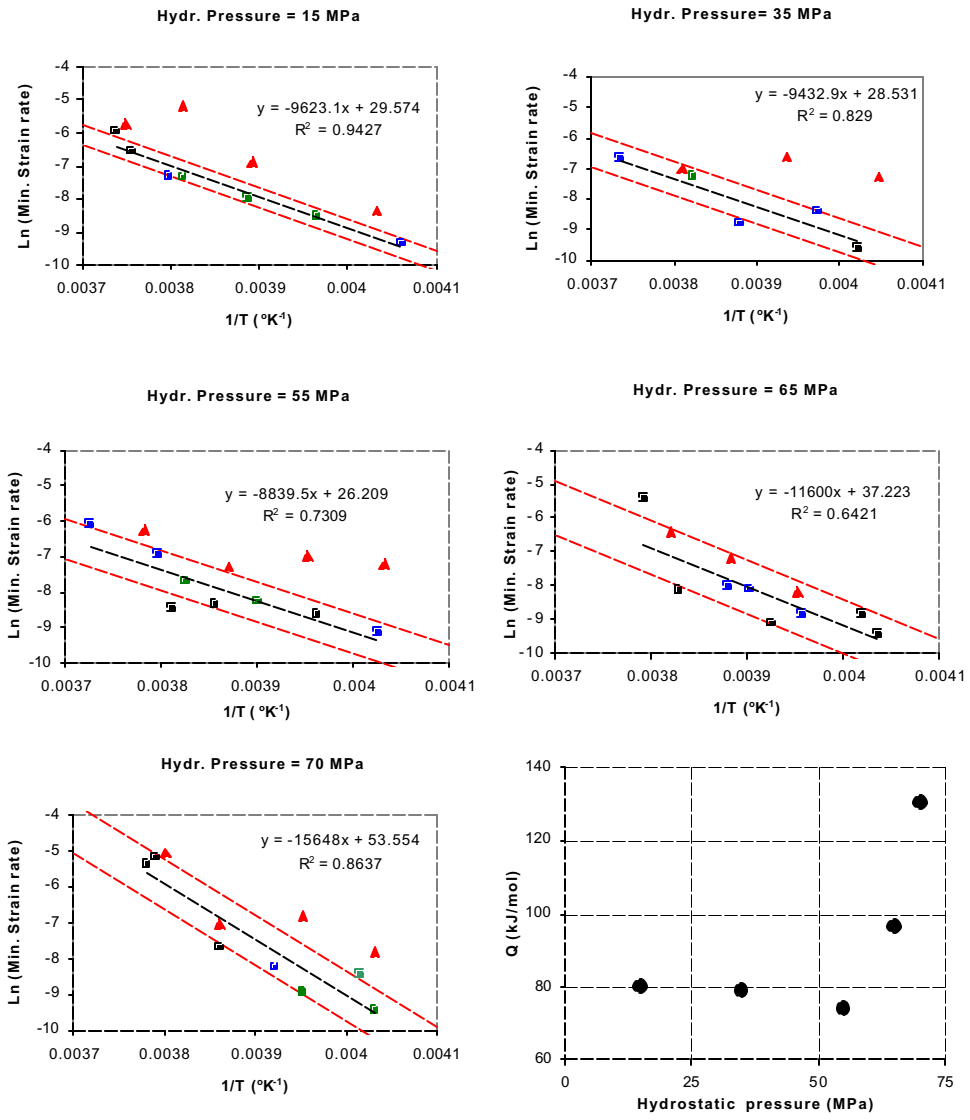

Figure 14: Plots of natural logarithm of minimum strain rate as a function of 1/T (deg. K) for five levels of hydrostatic pressure. The plot at the lower right is the variation of activation energy, determined from the linear regression on the five plots, with respect to the hydrostatic pressure. Square symbols are laboratory-made ice (black: normal seed, blue: coarse seed, green: air entrapment in specimen); Red triangles are tests with iceberg ice. Black lines are linear regression on results from tests with laboratory ice; red lines are a standard deviation above and below this regression.

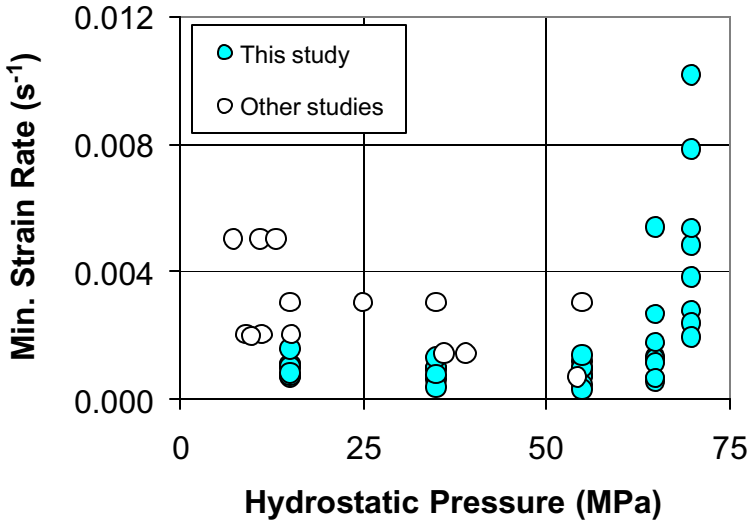

Figure 15: Plot of minimum strain rate as a function of hydrostatic pressure for all tests. The data is corrected for a temperature of -10°C with the linear regressions in Figure 14. The data from other studies (Jones 1982, Durham et al. 1983, Kalifa et al. 1989, Rist and Murrell 1994 and Mizuno 1998) were obtained from constant strain rate tests (see text).

5.3.2. Minimum strain rate and activation energy

Plots of the natural logarithm of the minimum strain rate as a function of 1/T ($^oK^{-1}$) are shown in Figure 14. Tests on both laboratory ice and iceberg ice are shown. An increase in temperature (towards the left on the x-axis) results in an increase in strain rate in all plots. No significant differences is seen between the three categories of laboratory ice (a larger number of tests would be required to verify this statement). The tests done with iceberg ice tend to have a higher minimum strain rate at a given temperature.

The activation energy was derived at each confinement level. This is shown in the lower right diagram of Figure 14. It shows a slight decrease in value at mid-range, followed by a drastic increase at the higher pressures. The results of all tests were corrected with the Arrhenius formulation for a temperature of –10°C, and are plotted in Figure 15. The strain rate appears to decrease slightly with increasing pressure and increases drastically upward of about 50 MPa. Test results for iceberg ice are also shown in Figure 16, and plotted together with the test results with laboratory ice in Figure 17. Overall, the minimum strain rate for iceberg ice is higher than that for laboratory ice.

The creep response of ice with a stress of 15 MPa was not found elsewhere in the open literature. Hence, a comparison between our test results and that of others was done with

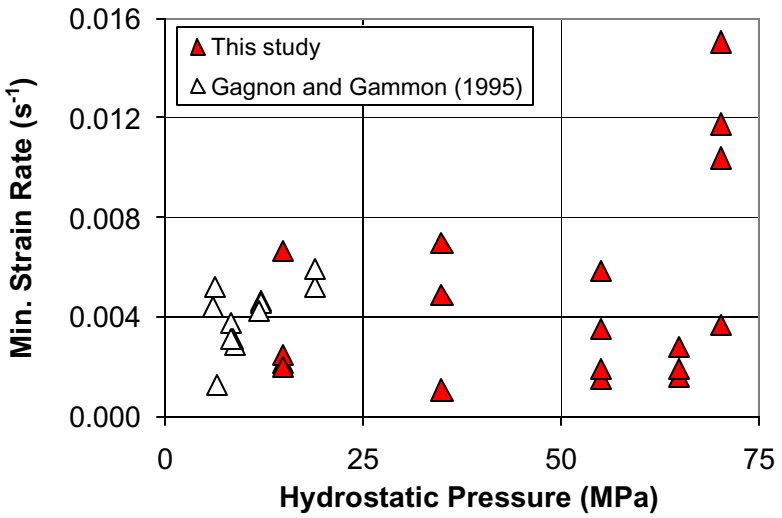

Figure 16: Plot of minimum strain rate as a function of hydrostatic pressure for all tests. The data is corrected for a temperature of -10°C with the linear regressions in Figure 14. The data from Gagnon and Gammon were obtained from constant strain rate tests (see text).

the information available on constant strain rate tests. Constant strain rate used for tests in other studies leading to an ultimate strength ranging between 14 and 16 MPa were gathered and plotted on Figure 15 and Figure 16. Most were done at the lower levels of hydrostatic stress. A reasonable agreement with our data is obtained. Figure 18 shows a similar trend for the accelerated creep (this data is part of an on-going damage analysis).

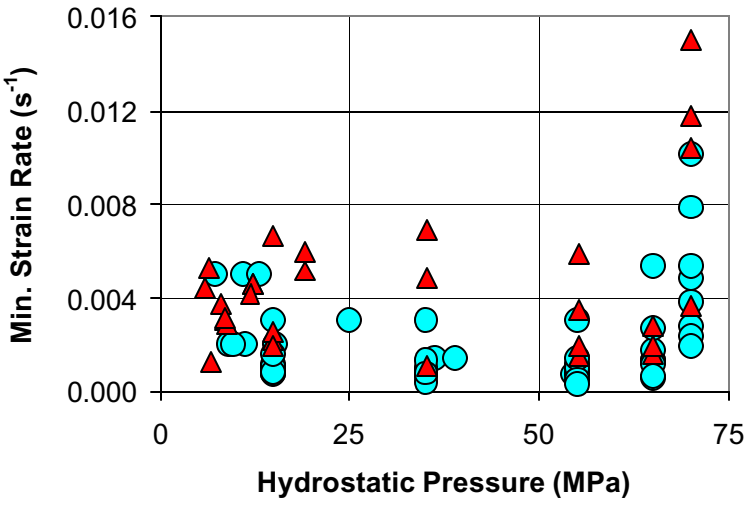

Figure 17:A combination of the plots shown in Figure 15 and Figure 16. Circles: Laboratory ice; Triangles: Iceberg ice.

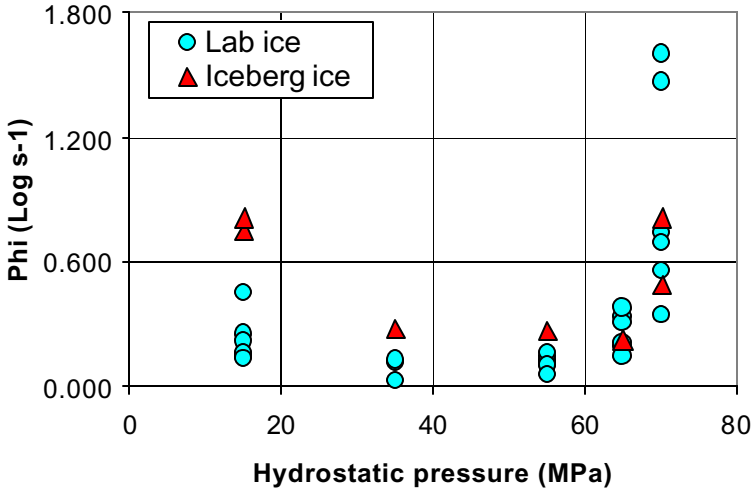

Figure 18: First slope(Phi) of accelerated creep (segment B in Figure 13) as a function of hydrostatic pressure. This also shows a trend similar to that found in Figure 17.

6. Summary

The following observations can be made from the results reported herein.

- Laboratory-made ice displays a slight decrease in minimum strain rate up to mid pressure levels but becomes significantly higher at high pressures, where it is characterized by a larger scatter. A similar trend was shown in other studies but it is here better defined for a pressure range believed to be representative of field conditions.

- The activation energy displays a small increase up to mid pressure range and increases substantially at the highest levels of hydrostatic pressure. The values for activation energy is in agreement with that documented in other studies. This trend in the values of the activation energy has not been documented elsewhere.

- Iceberg ice displays a larger scatter than laboratory-made ice and is generally weaker. It appears to have the same pressure and temperature dependency.

7. Implications for ice-structure interactions

These results reveal that the shearing resistance of ice is substantially lower at hydrostatic pressures exceeding 40 to 50 MPa. The radical increase in activation energy concurrent with the mechanical weakening of the ice points out to deformation mechanisms of a very different nature than those operating at lower levels of hydrostatic pressure. An increase in activation energy is also documented in ice towards its melting point at atmospheric pressure (Mellor and Testa 1969, Barnes et al. 1971, Mizuno 1992). This is attributed to the presence of liquid at grain boundaries. Similarly, when ice approaches its pressure melting point, melting is expected to occur along grain-boundaries, possibly at the junction of grains that are not favorably oriented for crystal slip. Recrystallization is another mechanism that is observed in ice deformed at higher levels of hydrostatic pressure (Meglis et al. 1999). This mechanism takes over the generation of microfractures, which predominates at the lower pressures.

The complex stress state existing in a floating ice feature, such as an iceberg, when it collides with an engineered structure involves a substantial degree of confinement and the development of high pressure zones (Jordaan et al. 1999, Jordaan 2001). These zones generate stresses up to 70 MPa (Frederking et al. 1990) – thus enabling the ice to puncture the hull of a ship. They are randomly distributed in space and are associated with a cyclical pattern of loading caused by repeated collapse within the zones. The work described in this report may indicate that the collapse of these zones is accompanied, and perhaps even controlled, by failure of the ice in the centre of the zone - where the hydrostatic pressure is highest.

The higher scatter of the data obtained from iceberg ice is expected, considering the inhomogeneous nature of this material. The use of good quality laboratory-produced ice

specimens may serve as an upper bound.

8. Future work

The use of minimum strain rate as a means of monitoring the relative compliance of the material provides an indication of its behaviour at a low level of strain. It may not be as relevant when trying to describe the deformation of the ice along the interface with an indentor, where it is believed to have undergone a significant amount of damage (Jordaan et al. 1999, Jordaan 2001). A better approach for this purpose is to address the deformation of ice at higher levels of strains (exceeding a few percent) and rely on state variables that retain a memory of previous deformation increments. This research is currently on-going. It will take into account the results of the testing programme described herein and will implement FEM algorithms to model numerically the deformational behaviour of ice under various loading conditions. It will follow-up on the work documented by Xiao and Jordaan (1996) and Jordaan et al. (1999). A new formulation will also be devised, that will take into account the effect of temperature and deviatoric stresses on the damage parameters.

9. References

Barnes P., Tabor D. and Walker J.C.F. 1971. The friction and creep of polycrystalline of ice. Proceedings of the Royal Society of London A324, 127-155.

Barrette P.D. 2001. Triaxial testing of ice: A survey of previous investigations. Proc. 16th Conference on Port and Ocean Engineering under Arctic Conditions (POAC), Ottawa, Vol. 3, 1375-1384.

Barrette P.D. and Jordaan I.J. 2001. Creep of ice and microstructural changes under confining pressure. In: S. Murakami and N. Ohno (eds.). IUTAM Symposium on Creep in Structures. Kluwer Academic Publ., Boston, 479-488.

Blair S.C. 1988. Mechanical properties of first-year sea ice at intermediate strain rates. Proc. POAC, vol. 3, 1-9.

Beeman M., Durham W.B. and Kirby S.H. 1988. Friction of ice. Journal of Geophysical Research 93, B7, 7625-7633.

Blair S.C. 1988. Mechanical properties of first-year sea ice at intermediate strain rates. Proc. POAC., Fairbanks, Alaska, Vol. 3, 1-9.

Boltz R.E. and Tuve G.L. 1970. Handbook of tables for applied engineering science. The Chemical Rubber Co., 975 pp.

Cole D.M. 1996. Observations of pressure effects on the creep of ice single crystals. Journal of Glaciology 42, 169-175.

Cox G.F.N and Richter-Menge J.A. 1988. Confined compressive strength of multi-year pressure ridge sea ice samples. Journal of Offshore Mechanics and Arctic Engineering 110, 295-301.

Durham W.B., Heard H.C. and Kirby S.H. 1983. Experimental deformation of polycrystalline H_2O ice at high pressure and low temperature: Preliminary results. Proc. 14th Lunar and Planetary Sci. Conf., Journal of Geophysical Research 88, Supplement, B377-B392.

Durham W.B., Stern L.A and Kirby S.H. 1996. Rheology of water ices V and VI. Journal of Geophysical Research 101, B2, 2989-3001

Frederking R.M.W. 1977. Plane strain compressive strength of columnar-grained and granular snow-ice. Journal of Glaciology 18, 505-516.

Frederking R.M.W., Jordaan I.J. and McCallum J.S. 1990. Field Tests of Ice Indentation

at Medium Scale Hobson's Choice Ice Island. IAHR Ice Symp. 931-944.

Gagnon R.E., Kiefte H., Clouter M.J., Whalley E. 1988. Pressure dependence of the elastic constants of ice Ih to 2.8 kbar by Brillouin Spectroscopy. Journal of Chemical Physics 89, 4522-4528.

Gagnon R.E. and Gammon P.H. 1995. Triaxial experiments on iceberg and glacier ice. Journal of Glaciology 41, 528-540.

Gagnon R.E. and Molgaard J. 1991. Evidence for Pressure Melting and Heat Generation By Viscous Flow of Liquid in Indentation and Impact Experiments on Ice. Annals of Glaciology 15. 254-260.

Gold L.W. 1973. Activation energy for creep of columnar-grained ice. In: E.Whalley, S.J. Jones and L.W. Gold (eds.), Physics and Chemistry of ice, Royal Society of Canada, Ottawa, 362-364.

Golubov A.I., Razbegin V.N. and Slepak M.E. 1990. Multiaxial creep of saline ice. Proc. 1st European Offshore Mechanics Symp., Trondheim, Norway, 556-561

Goughnour R.R. and Andersland O.B. 1968. Mechanical properties of a sand-ice system. Journal of Soil Mechanics and Foundations Division, Proc. American Society of Civil Engineering SM-4, 923-950.

Gratz E.T. and Schulson E.M. 1997. Brittle failure of columnar saline ice under triaxial compression. Journal of Geophysical Research 102, B3, 5091-5107.

Haefeli R., Jaccard C. and De Quervain M. 1968. Deformation of polycrystalline ice under combined uniaxial and hydrostatic pressure. International Union of Geodesy and Geophysics, International Association of Scientific Hydrology, General Assembly of Bern 1967, Publication # 79, 341-344.

Haüsler F.U., Matthies H.G. and Moore C.S. 1991. Sea ice under complex stress states: Constitutive modelling and testing. In: S.Jones, R.F. McKenna, J. Tillotson and I.Jordaan (Eds.) Ice-Structure Interactions. Proc. IUTAM-IAHR Symp., St.John's, Springer-Verlag, Berlin, 363-381.

Haynes F.D. 1973. Tensile strength of ice under triaxial stresses. CRREL report RR 312.

Hobbs P.V. 1974. Ice Physics. Clarendon Press, Oxford, 837 pp.

Homer D.R. and Glen J.W. 1978. The creep activation energies of ice. Journal of Glaciology 21, 429-443.

Jones S.J. 1978. Triaxial testing of polycrystalline of ice. In: Proc. 3rd Int. Conf. Permafrost, Edmonton, Vol. 1, 671-674.

Jones S.J. 1982. The confined compressive strength of polycrystalline ice. Journal of Glaciology 28, 171-177.

Jones S.J. and Chew A.M. 1983. Creep of ice as a function of hydrostatic pressure. Journal of Physical Chemistry 87, 4064-4066.

Jordaan I.J., Matskevitch D.G. and Meglis I.L. 1999. Disintegration of Ice Under Fast Compressive Loading. International Journal of Fracture 97. 279-300.

Jordaan I.J. 2001. Mechanics of ice-structure interaction. Engineering Fracture Mechanics 68, 1923-1960.

Kalifa P., Duval P. and Ricard M. 1989. Crack nucleation in polycrystalline ice under compressive stress states. Proc. 8th OMAE Conf., vol. 4, The Hague, 13-21.

Kalifa P., Ouillon G., Duval P. 1992. Microcracking and the failure of polycrystalline ice under triaxial compression. Journal of Glaciology 38, 65-76.

Kirby S.H., Durham W.B. and Heard H.C. 1985. Rheologies of H_2O ices I_h, II and III at high pressures: A progress report. In: J. Klinger, D. Benest, A. Dollfus and R. Smoluchowski (eds), Ices in the Solar System, D. Reidel Publ. Comp., Hingham, MA, 89-107.

Mae S. and Azuma N. 1989. Ice sheet dynamics and rheology of ice under hydrostatic pressure. In: S. Karato and M. Toriumi (Eds.), Rheology of solids and of the Earth, Oxford University Press, N.Y. 209-222.

Masterson D.M., Nevel D.E., Johnson R.C., Kenny J.J. and Spencer P.A. 1992. The medium scale iceberg impact test program. In : Proc. IAHR Ice symposium, Banff, Alberta, 930-953.

Masterson D.M., Spencer P.A., Nevel D.E. and Nordgren R.P. 1999. Velocity Effects from Multi-Year Ice Tests. In : Proc. 18th Conf. on Offshore Mechanics and Arctic Engineering. St.Johns, Newfoundland, 1-27.

Meglis I.L., Melanson P.M. and Jordaan I.J. 1999. Microstructural change in ice: II. Creep behavior under triaxial stress conditions. Journal of Glaciology 45, 438-448.

Melanson P.M., Jordaan I.J. and Meglis I.L. 1999a. Modelling of damage in ice. In: H.T Shen (Ed.). Ice in surface waters. Proc. 14th Int. Symp. On Ice, A.A. Balkema, Brookfield, 979-988.

Melanson P.M., Meglis I.L., Jordaan I.J. and Stone B.M. 1999b. Microstructural change in ice :I. Constant-deformation-rate tests under triaxial stress conditions. Journal of Glaciology 45, 417-422.

Mellor M. 1980. Mechanical properties of polycrystalline ice. In: Tryde P. (ed.) Physics

and mechanics of ice. Springer-Verlag. Berlin.

Mellor M. and Cole D.M. 1982. Stress/Strain/Time relations for ice under uniaxial compression. Cold Regions Science and Technology 6, 207-230.

Mellor M. and Cole D.M. 1983. Deformation and failure of ice under constant stress or constant strain- Cold Regions Science and Technology 5, 201-219.

Mellor M. and Testa R. 1969. Effect of temperature on the creep of ice. Journal of Glaciology 8, 131-145.

Melton J.S. and Schulson E.M. 1995. Preliminary results on the ductile deformation of columnar saline ice under triaxial compressive loading. Proc. 14th OMAE Conf., Copenhagen, Vol. 4, 139-143.

Melton J.S. and Schulson E.M. 1997. The ductile deformation of columnar (S2) saline ice under triaxial compression. Proc. 7th ISOPE Conf., Honolulu, Vol. 2, 402-409.

Melton J.S. and Schulson E.M. 1998a. A comparison of the ductile compressive strength of columnar saline ice under proportional and conventional triaxial loading. Proc. 8th ISOPE Conf., Montréal, Vol. 2, 408-415.

Melton J.S. and Schulson E.M. 1998b. Ductile compressive failure of columnar saline ice under triaxial loading. Journal of Geophysical Research 103, C10, 21759-21766.

Metcalfe H.C., Williams J.E. and Castka J.F. 1974. Modern Chemistry. Holt, Rinehart and Winston, Toronto, 657 pp.

Mizuno Y. 1992. High temperature creep of polycrystalline ice under hydrostatic pressure. In: N. Maeno and T. Hondoh (Eds.), Physics and Chemistry of Ice, Hokkaido University Press, Sapporo, 434-439.

Mizuno Y. 1998. Effect of hydrostatic confining pressure on the failure mode and compressive strength of polycrystalline ice. Journal of Physical Chemistry B, 102, 376-381.

Muggeridge K.J. and Jordaan I.J. 1999. Microstructural Change in Ice :III. Observations From an Iceberg Impact Zone. Journal of Glaciology.45, 449-456.

Murrell S.A.F., Sammonds P.R. and Rist M.A. 1991. Strength and failure modes of pure ice and multi-year sea ice under triaxial loading. In: S.Jones, R.F. McKenna, J. Tillotson and I.Jordaan (eds.) Ice-Structure Interactions. Proc. IUTAM-IAHR Symp., St.John's, Canada, Springer-Verlag, Berlin, 339-361.

Nadreau J.P and Michel B. 1986a. Secondary creep in confined ice samples. Proc. 8th IAHR Ice Symp., Iowa City, Iowa, Vol. 1, 307-318.

Nadreau J.P and Michel B. 1986b. Yield envelope for confined ice. Proc. 1st Int. Conf.

Ice Technology, 25-36.

Nadreau J.P., Nawwar A.M. and Wang Y.S. 1991. Triaxial testing of freshwater ice at low confining pressures. Journal of Offshore Mechanics and Arctic Engineering 113, 260-265.

Nawwar A.M., Nadreau J.P. and Wang Y.S. 1983. Triaxial Compressive Strength of Saline Ice. In : Proc. 7th inter. conf. on port and ocean engineering under arctic conditions, Vol.3. 193-201.

Nemat-Nasser S. 2000.. ASM Handbook, Vol. 8, Mechanical Testing and Evaluation. ASM International, Materials Park, Ohio.

Nordell B. 1990. Measurement of P-T coexistence curve for ice-water mixture. Cold Regions Scicence and Technology 19, 83-88.

Panov V.V. and Fokeev N.V. 1981. Compression strength of sea ice specimens under complex loading. In: A.F. Treschnikov (Ed.) Problems of the arctic and Antarctic, Division of Polar Programs, National Science Fondation, Washington, DC., Vol. 49, 97-104.

Paterson W.S.B. 1999. Some aspects of the physics of glaciers. In: J.S. Wettlaufer, J.G. Dash, N. Untersteiner, Ice Physics and the Natural Environment. NATO ASI Series 1: Global Environmental Change, Vol. 56, p. 69.

Popov E.P. 1990. Engineering mechanics of solids. Prentice-Hall, Toronto, 727 pp.

Poirier J.P. (1985) Creep of crystals – High-temperature deformation processes in metals, ceramics and minerals. Cambridge University Press, 260 pp.

Richter-Menge J.A. 1991. Confined compressive stength of horizontal first-year sea ice samples. Journal of Offshore Mechanics and Arctic Engineering 113, 344-351.

Rigsby G.P. 1958. Effect of hydrostatic pressure on velocity of shear deformation of single ice crystals. Journal of Glaciology 3, 273-278.

Rist M.A. 1997. High-stress ice fracture and friction. Journal of Physical Chemistry B 101, 6263-6266.

Rist M.A. and Murrell S.A.F. 1994. Ice triaxial deformation and fracture. Journal of Glaciology 40, 305-318.

Rist M.A.,Murrell S.A.F. and Sammonds P.R. 1988. Experimental results on the failure of polycrystalline ice under triaxial stress conditions. Proc. IAHR, Sapporo, Japan, 118-127.

Rist M.A, Jones S.J. and Slade T.D. 1994. Microcracking and shear fracture in ice. Annals

of Glaciology 19, 131-137.

Sammonds P.R. and Murrell S.A.F. 1989. A laboratory investigation of the fracture of multi-year sea ice under triaxial stresses at -20C and -40C. Proc. 10th POAC Conf., Luleå, Vol. 1, 279-288.

Sammonds P.R., Murrell S.A.F. and Rist M.A. 1998. Fracture of Multiyear Sea Ice. Journal of Geophysical Research 103, #C10. 21795-21815.

Schulson E.M., Gies M.C., Lasonde G.J. and Nixon W.A. 1989. The effect of the specimen-platen interface on internal cracking and brittle fracture of ice under compression: high-speed photography. Journal of Glaciology 35, 378-382.

Schulson E.M. and Gratz E.T. 1999. The brittle compressive failure of orthotropic ice under triaxial loading. Acta Materialia 47, 745-755.

Schulson E.M., Jones D.E., Kuehn G.A. 1991. The effect of confinement on the brittle compressive fracture of ice. Annals of Glaciology 15, 216-221.

Simonson E.R., Jones A.H. and Green S.J. 1975. High pressure mechanical properties of three frozen materials. Fourth International Conference on High Pressure, Kyoto, International Association for the Advancement of High Pressure Science and Technology, Physico-Chemical Society of Japan, Kyoto, 115-121.

Sinha N.K. 1979a. Effect of Test System Stiffness on Strength of Ice. Proc. POAC. 708-717.

Sinha N.K. 1979b. Grain boundary sliding in polycrystalline materials. Philosophical Magazine A, 40, 825-842.

Sinha N.K. 1981a. Comparative study of ice strength data. Proc. IAHR Int. Symp. on Ice. Quebec, vol. 2, 581-595.

Sinha N.K. 1981b. Rate sensitivity of compressive strength of columnar grained ice. Experimental Mechanics 21, 209-218.

Sinha N.K. 1984a. Intercrystalline cracking, grain-boundary sliding, and delayed elasticity at high temperatures. Journal of Materials Science 19, 359-376.

Sinha N.K. 1984b. Uniaxial compressive strength of first-year and multi-year sea ice. Canadian J. Civil Engineering 11, 82-91.

Sinha N.K., Zhan C. and Evgin E. 1995. Uniaxial Constant Compressive Stress Creep Tests on Sea Ice. Journal of Offshore Mechanics and Arctic Engineering 117. 283-289.

Stone B.M., Jordaan I.J., Jones S.J. and McKenna R.F. 1989. Damage of isotropic polycrystalline ice under moderate confining pressures. Proc. POAC Conf., Luleå, Vol. 1,

408-419.

Stone B.M., Jordaan I.J., Xiao J. and Jones S.J. 1997. Experiments on the damage process in ice under compressive states of stress. Journal of Glaciology 43, 11-25.

Timco G.W. and Frederking R.M.W. 1986. Confined Compression Tests : Outlining the Failure Envelope of Columnar Sea Ice. Cold Regions Science and Technology 12, 13-28.

Weiss J. and Schulson E.M. 1995. The failure of fresh-water granular ice under multiaxial compressive loading. Acta Metallurgica et Materialia 43, 2303-2315.

Xiao J. and Jordaan I.J. 1996. Application of damage mechanics to ice failure in compression. Cold Regions Science and Technology 24, 305-322.

Appendix 1

Previous investigations on the triaxial testing of ice, arranged in chronological order by date of reference

Investigator(s)	Ice type	Test	Max. P_c (MPa)	Max. Dev. (MPa)	Log_{10} strain rate (s^{-1})	Temp. (^oC)	Observations
Rigsby 1958	L,M,F	CS	31	0.26		-20 to -1	A higher temperature leads to higher shear strain rate. The latter is independent of hydrostatic pressure for a given difference between ice temperature and melting point.
Goughnour and Andersland 1968	L,P,F	CR	0.7		-3.9, -3.6	-12, -4	Strength increases with pressure at high strain rates, but varies little at the lower rate. Effect of load history investigated.
Haefeli et al. 1968	L,P,F	CS	30	0.08		-8.1 to -5.9	Higher confinement leads to higher creep rate of granular ice for a given ice temperature. This rate decreases again upon decrease in temperature equivalent to depression of pressure melting point.
Haynes 1973	L,G,F		0.2		-5	-7	Tensile strength tests. Axial stress delivered by confinement medium. Various confinement/axial stress ratios used. Yield stress decreases with increase in ratio.
Simonson et al. 1975	L,P	CR	200[(ii)]		-4 to 0	-10	Increase in strength with increasing strain rate. Decrease in strength with increase in hydrostatic pressure. Increase of pressure alone (no deviator) induces reduction in porosity, decrease in Young's modulus and melting of ice at 100 MPa.
Jones 1978, 1982	L,G,F	CR	85		-5.9 to -1.9	-12	Strength increases up to 25-30 MPa confinement but decreases slightly with further increase in confinement. This trend is more evident for higher strain rates. Stress exponent higher for unconfined than for confined. Confinement induces ductile (as opposed to brittle) deformation.
Panov and Fokeev 1981	L,P,S / N,S		12[(i)]	20		-23 to -1.9	Strength increases with confinement. Confinement is a ratio of axial loading.

Haüsler 1981	L,C,S	CR	(iii)		-3.7	-10	Strength vs stress ratios, and projection of a failure surface.
Jones and Chew 1983	L,G,F	CS	60	0.47		-10	Minimum creep rate is lowest at 15 MPa confinement then increases upon further increase in confinement. Activation volume discussed.
Durham et al. 1983	L,G,F	CR	350		-5.5 to -3.5	-196 to -15	Mapped brittle-ductile transition. Strength of granular ice increases with confinement at both end of temperature scales to confinements of 50 MPa. It then levels (for brittle behaviour) or drops (ductile behaviour) at higher confinements. Low temperature causes strength to increase. Enthalpy variation with temperature.
Nawwar et al. 1983	L,C,S	CR	2.8		-5.3 to -1.2	-2 to -20	Linear dependency of strength on confining pressure above 1MPa. At a confinement of 2.8 MPa the strength is about 2.3 times the uniaxial strength.
Kirby et al. 1985	L,G,F	CR	50		-6.5 to -2.5	-120 to -5	Identification of three flow regimes at different temperature intervals. Variation in activation energy discussed.
Nadreau and Michel 1986a,b	L,G,F / L,G,S / I	CR, CS	70	not provided	-6 to -4	-20,-10, -5, -3	Glen's exponent *n* decreases with increase in confinement. Increase of maximum shear stress up to 15-20 MPa confinement followed by decrease at higher confinement.
Blair 1988	1Y	CR	50		-2 to 3.3	-20 to -8	Axial strain as a function of hydrostatic pressure. Strength increases with mean stress up to 7.5 MPa and levels off at a higher confinement. Decrease in strength from $10^{-2}s^{-1}$ to 0.5 $s^{-1}$and levelling off at higher strain rate.
Rist et al. 1988	L,G,F	CR	30		-4, -3, -2	-20	Variation of failure mode with confinement. Strength increases with confinement for all strain rates.
Beeman et al. 1988	L,G,F	CR	250		-3.8, -2.7, -1.7	-196, -183, -158	Investigations of friction on 45 deg. saw cuts surfaces. $\mu = 0.55$ and 0.20 below and above 10 MPa, respectively, of confining pressure. Independent of temperature and average

							sliding velocity.
Sammonds and Murrell 1989, Sammonds et al. 1989	>1Y	CR	30		-6 to -2	-40, -20, -10	Modes of failure described. Comparison of data with failure surfaces. Pressure dependence of fracture strength only for lowest temperature.
Cox and Richter-Menge 1988	>1Y	CR	20[(i)]		-5, -3	-20, -5	Constant ratio between radial and axial stress. Classification of stress-strain curves. Strength increases with increase in confinement and strain rate, and decreasing temperature.
Kalifa et al. 1989	L,G,F	CR	10		-4.6 to -3	-10	Confinement increases the deviatoric stress level and the strain when the first crack is observed. The cracks tend to form parallel to the largest stress deviator. Intra- vs intercrystalline cracks investigated.
Stone et al. 1989	L,G,F	CR,D	5		-4.3, -4, -3	-10	Damage, defined as change in apparent elastic moduli, is increased by confinement. Flow stress decreases and stabilises with repeated loading.
Mae and Azuma 1989	M,F / P,F		56[(ii)]		-7	-20 to -5	Stress relaxation tests on crystals. Activation volume. Effect of hydrostatic pressure on flow law of polycrystalline ice. Hydrostatic stress hardens crystals but softens polycrystals.
Golubov et al. 1990	L,P,S	CS	7[(ii)]	2.4		-5	Both strength (but not CR) and creep tests reported. Strength increases by a factor of 2.5 from lowest to highest hydrostatic pressure. Increase in creep rate with decrease in pressure. Volume strains discussed. Visco-elastic theory presented.
Richter-Menge 1991	1Y	CR	20[(i)]		-5, -3	-10	Constant ratio between radial and axial stress. Stress exponent not affected by confinement. Strength, strain at failure and initial tangent modulus increase with confinement for all orientation of columnar grained specimens. Classification of stress-strain curves.
Nadreau et al.	L,C,F	CR	2.85		-5.5 to	-20, -10,	Specimens cut parallel, perpendicular and at an angle with the

1991					-1.4	-2	columnar structure. Strength increases with confinement and strain rate. Tear drop failure envelope discussed.
Schulson et al. 1991	L,G,F	CR	(iii)		-3	-40	Fracture stress increases with confinement ratio. Brittle mechanisms discussed and cracking mechanism presented.
Murrell et al. 1991	L,G,F / >1Y	CR	30		-5 to -2	-40, -20, -10	Brittle and ductile failure described, through specimen yield mode and acoustic emission. Increase in strength with confining pressure (up to 10-15 MPa) is more significant at higher strain rate.
Mizuno 1992	L,G,F	CS	35	3		-10 to -0.8	Accelerating creep, grain growth and preferred crystal orientation followed by strain rate reduction and grain refinement. Interpretation of minimum creep rate in terms of homologous temperature. Activation enthalpy is higher above -6^{o}C and for higher pressure.
Kalifa et al. 1992	L,G,F	CR,D	10		-5.2 to -2.3	-10	Crack density decreases and peak stress and corresponding strain increase with confinement. At higher strain rates, the strength of ice decreased with increase in grain size. Relative contribution of elastic strain to total strain is reduced at higher confinement assuming damage does not affect elastic modulus.
Rist and Murrell 1994	L,G,F	CR	46		-5 to -2	-40 to -5	Cracking activity mapped as a function of confinement and strain rate. At high strain rate, strength increases up to 10 MPa confinement, above which it becomes pressure-independent. At low strain rate, it is mostly pressure independent. Failure modes, activation energy and friction.
Rist et al. 1994	L,G,F	CR,D	30		-4, -2	-20	Shear fracture strength weakly dependant on confinement. Crack sliding not observed. No effect of damage on fracture strength. Pressure prevents cracking and reduce post-failure drop, despite 4^{o}C decrease in pressure-melting point.
Gagnon and	I	CR	14		-4.3 to -	-16 to -1	Variation of failure mode mapped with pressure-strain rate.

Gammon 1995					1.3		Strength increases with decreasing temperature, increasing strain rate up to $5x10^{-3}$ s^{-1}, and increase in confinement at lower temperatures. Friction and activation energy discussed.
Weiss and Schulson 1995	L,G,F	CR	(iii)		-3	-40, -20, -10	Brittle to 'pseudo'-ductile failure of granular ice ice under various loading configurations. At low confinement, failure stress increases with confinement. Role of boundary conditions in ice failure at high confinement. Failure stress related to the boundary conditions.
Cole 1996	L,M,F	CS	19	0.33		-10	Small variations of steady-state strain rate with axial load and pressure.
Rist 1997	L, M / L,G	CR	20		-3, -2	-20, -10	Elastic-brittle failure mode of crystals with different orientations and polycrystals. Correspondence of shear and normal stresses. Frictional sliding along yield surfaces investigated.
Gratz and Schulson 1997	L,C,S	CR	(iii)		-2.2	-10	Brittle failure of columnar grained ice under various loading configurations. Three regimes of behaviour described. High sensitivity of strength to confining stress. Frictional cracking mechanisms.
Stone et al. 1997	L,G,F	CS, CR, D	20	7.65	-4	-10	Confinement suppresses cracking in favour of recrystallisation and void formation. Creep enhancement due to damage more important when damage done under triaxial conditions. Pressure reduction leads to increase in deformation.
Melton and Schulson 1995, 1997, 1998a,b	L,C,S	CR	(iii)		-4.4	-10	Ductile failure of columnar grained ice under various loading configurations. Strength independent of along-column confinement under small across column confinement but increases with along column stress at high across column confinement.
Mizuno 1998	L,G,C,	CR	50		-3.5 to -	-11	Peak in strength at mid-confinement for high strain rate. This

	F				1.3		peak increases with strain rate and grain size. Internal structure discussed.
Sammonds et al. 1998	>1Y	CR	30		-6.3 to -2	-40 to -3	Failure modes. Pressure dependency of failure modes across brittle-ductile transition. Frictional sliding investigated. Shear fracture weakly pressure dependant at -20^{o}C and above, stronger dependency at -40^{o}C up to 14 MPa confinement. Fracture toughness investigated.
Melanson et al. 1999a	L,G,F	CS, D	60	24		-10	High strains achieved to investigate tertiary creep behaviour. Deformation described by a damage parameter whose rate decreases at mid pressure range and increases again at higher pressure. Constitutive model presented.
Schulson and Gratz 1999	L,C,F	CR	(iii)		-2.2	-10	Brittle failure of columnar grained ice studied with various loading configurations. Similar mechanisms to those observed in saline ice at same conditions (Gratz and Schulson 1997).'Splay' cracking mechanism described.
Melanson et al. 1999b	L,G,F	CR	20		-4, -2	-10	Higher peak stress at high strain rate. Reduction of grain size observed between strain at failure and 3-5% strain, stabilises upon further deformation.
Meglis et al. 1999	L,G,F	CS,D	60	25		-10 to -8	Stress exponent independent of confinement and strain level. Viscosity decreases with strain up to 44%. Microcracking and dynamic recrystallization predominate at low and high confinement, respectively. Characterisation of microstructure with strain and confinement.
Barrette and Jordaan 2001	L,C,F	CS	70	30		-10	Viscoelastic compliance highest at low and high pressure ranges, with a minimum in between. The morphology of shear fractures at low and high confinement is compared.

(i) Estimated. (ii) Hydrostatic (mean) stress. (iii) Multiaxial, brush-type platens

Appendix 2

Photography of ice specimens and internal structure

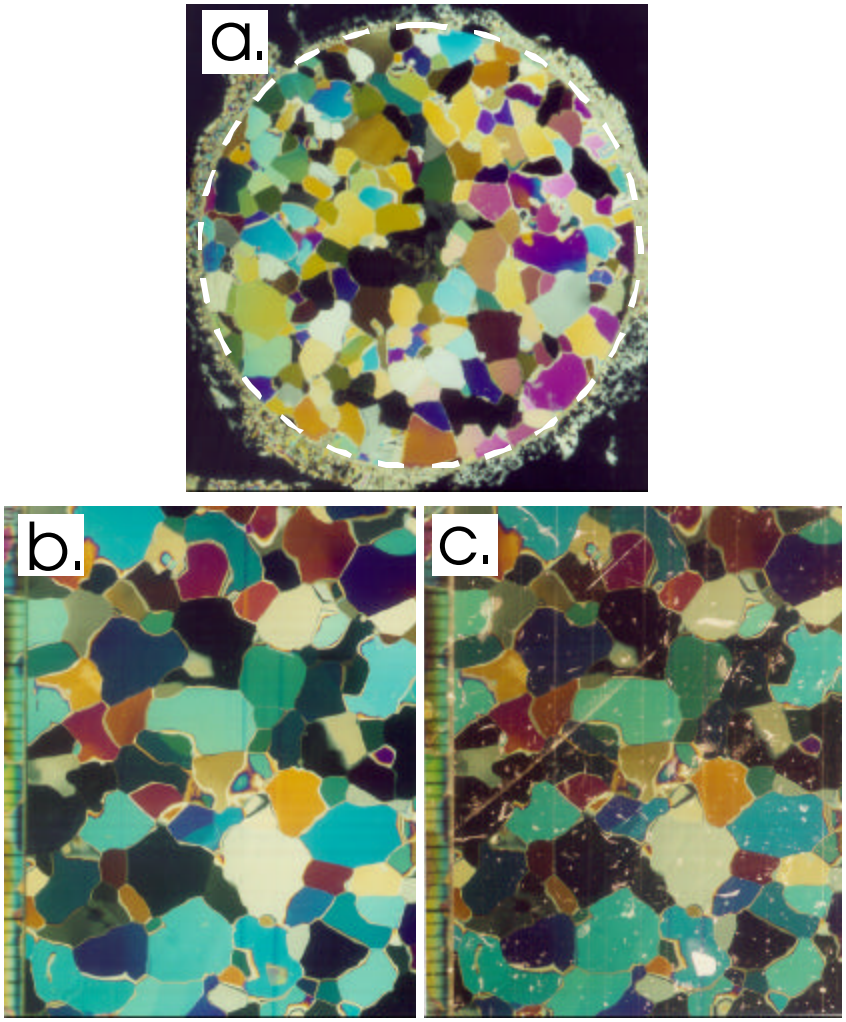

Figure 19: Thin sections of laboratory-grown ice. a) Cross section of a cylindrical specimen viewed under crossed-polarized light. The section is 70 mm in diameter. The dashed line separates the ice in the specimen from the ice used to weld the section onto the underlying glass plate. b) Another example at larger scale and under the same light conditions (scale in mm). c) Same as in (b), but with the addition of side (reflected) light, showing few internal defects such as air entrapment in the form of bubbles, fractures, etc..

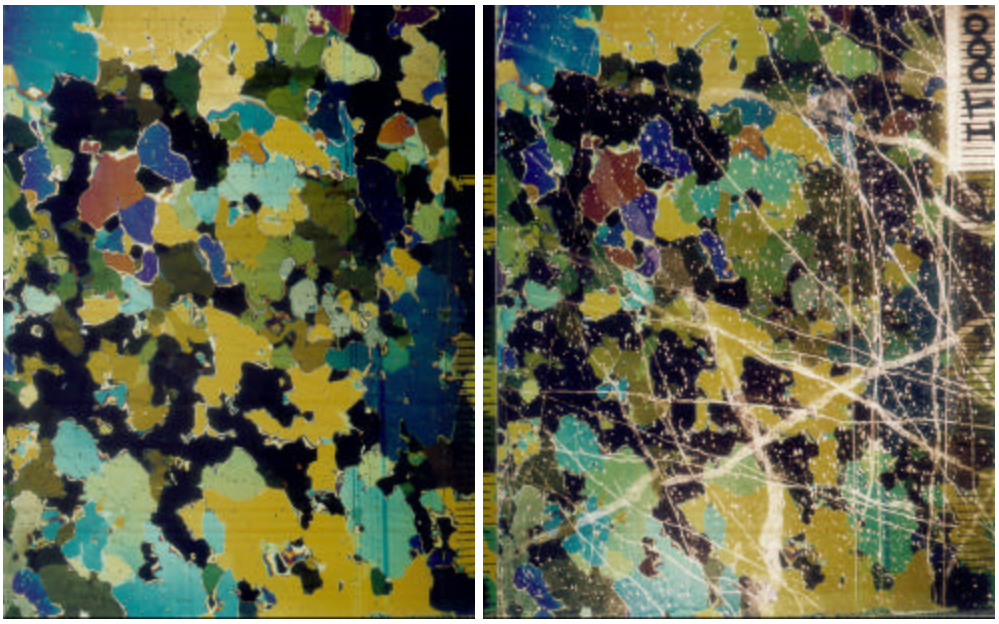

Figure 20: Thin sections of undeformed iceberg ice viewed under cross-polarized light (left) and with the addition of side (reflected) light (right)(scale in mm). Note the abundance of sub-millimetre size air inclusions and various sets of linear (planar in three dimensions) features. The crystals display a wide range in size (unlike in laboratory-grown ice – compare with Figure 19) and serrated boundaries.

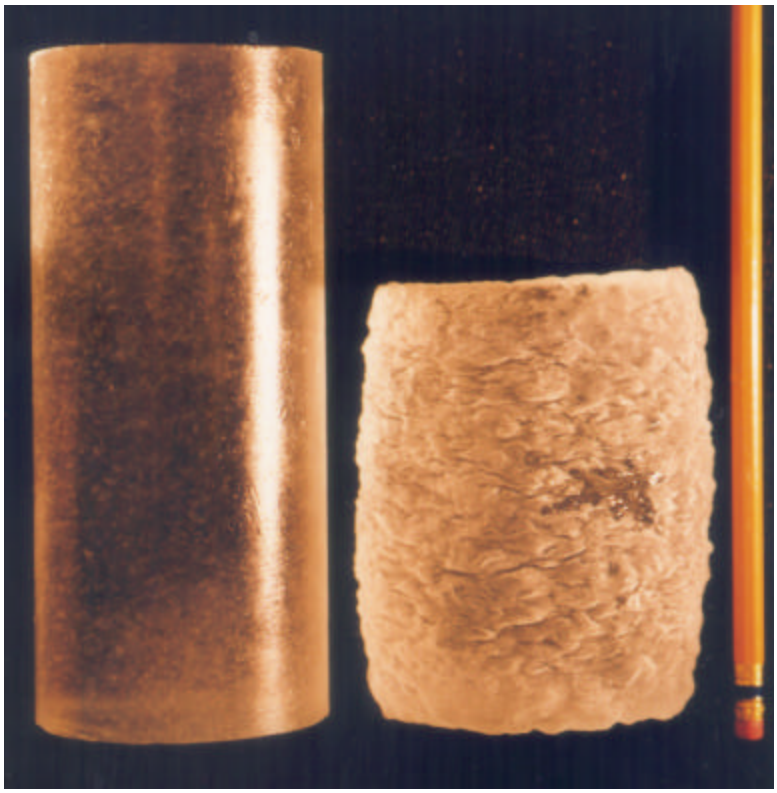

Figure 21: Ice specimens made from laboratory-produced ice. Initial size for all specimens (both this ice and iceberg ice) was 155 mm in length and 70 mm in diameter (the pencil is for scale). Left, undeformed; right, deformed to 33% true strain at 50 MPa confinement and –10°C. Note the final barrel-shape configuration.

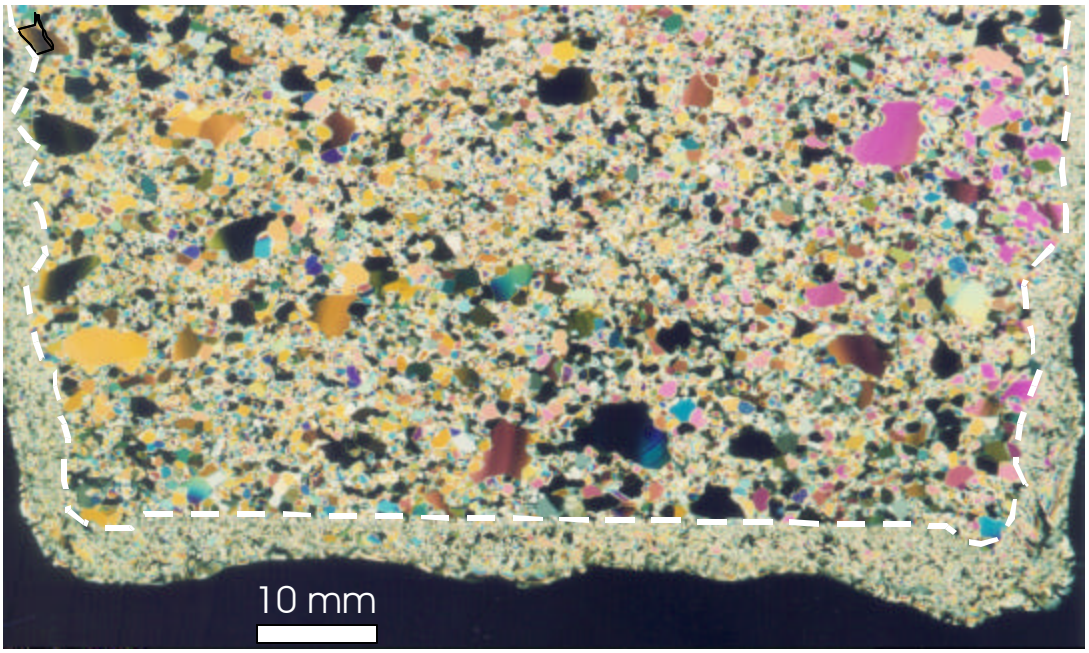

Figure 22: Thin section of deformed specimen shown in Figure 21 (part thereof). The dashed line separates the ice in the specimen from the ice used to weld the section onto the underlying glass plate. The internal structure is characterized by a strong recrysallization texture. The nature of the corrugations at the specimen's surface is displayed.

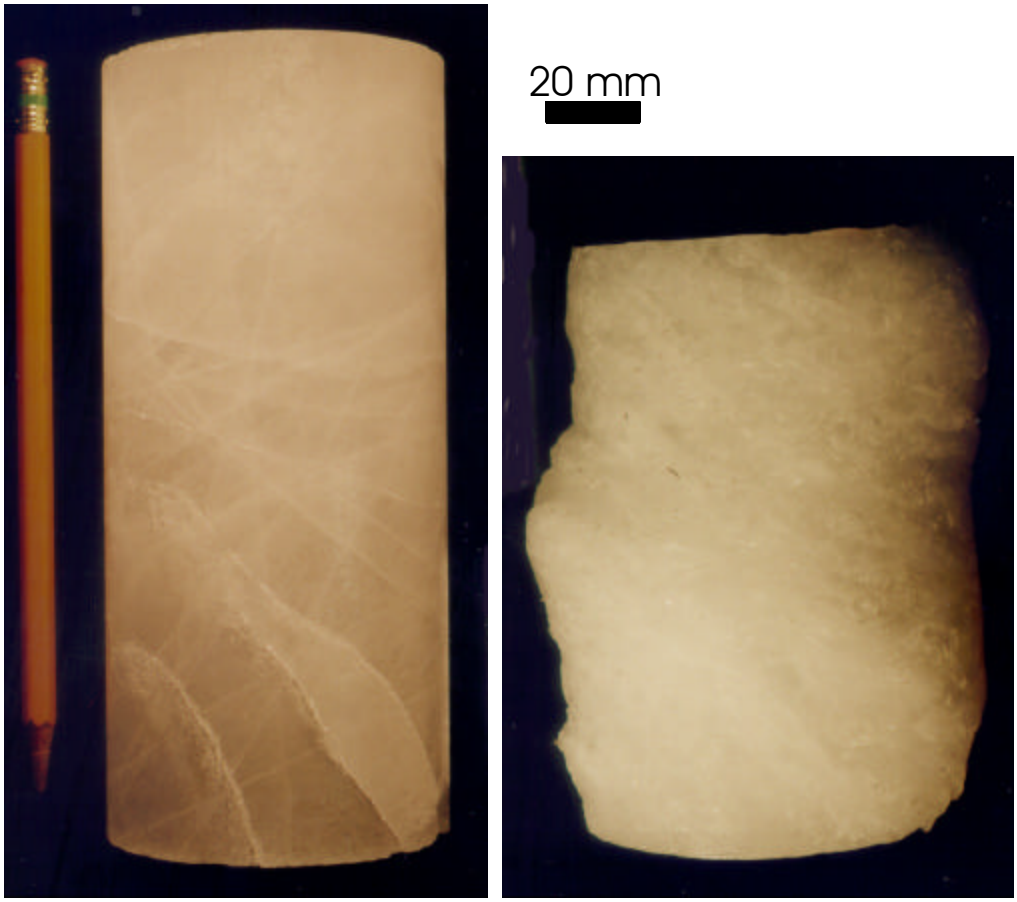

Figure 23: Ice specimens made from iceberg ice. Left, undeformed; right, deformed to 27% true strain at 7 MPa confinement (-10°C). Note the 'flaw' pattern in the undeformed specimen and the inhomogeneous nature of the deformation. The chalky white colour is indicative of widespread microcracking. Unlike the example shown in Figure 27, these flaws did not cause the ice to rupture.

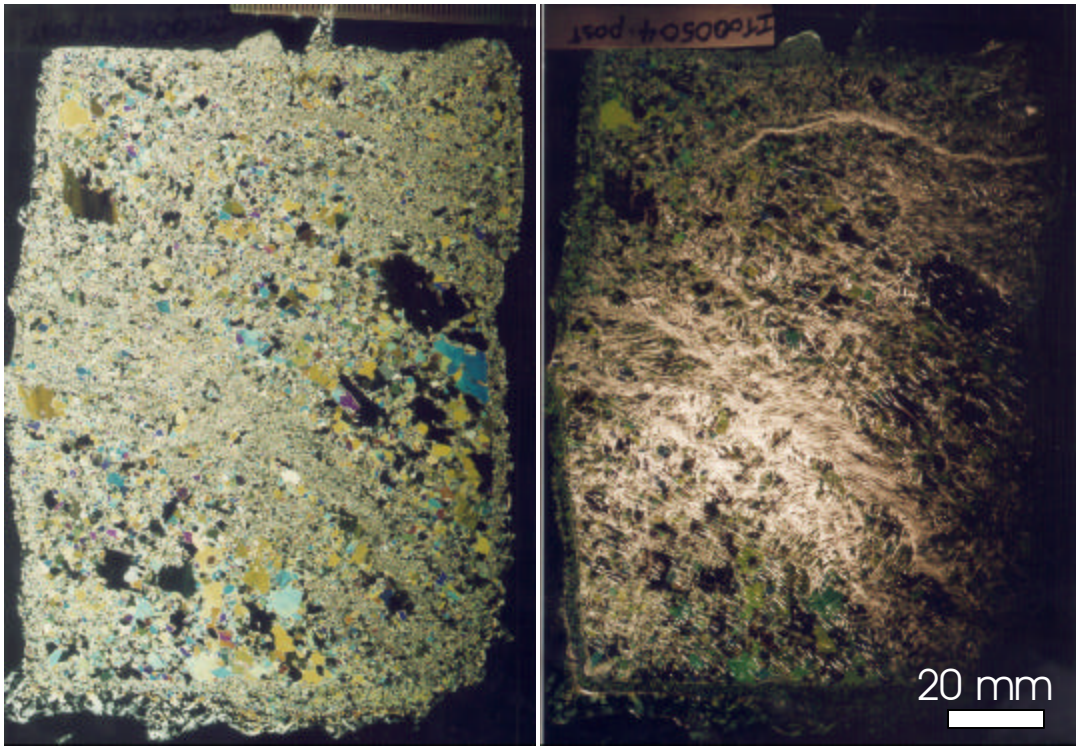

Figure 24: Thin section of the specimen shown inFigure 23. Left: Transmitted light only; right, side (reflected) light only of the central portion, showing intense cracking pattern. Grain refinement occurs in a 'band' located in the centre of the specimen, dipping about 45 deg. to the right from the horizontal (this feature may also be observed in the specimen).

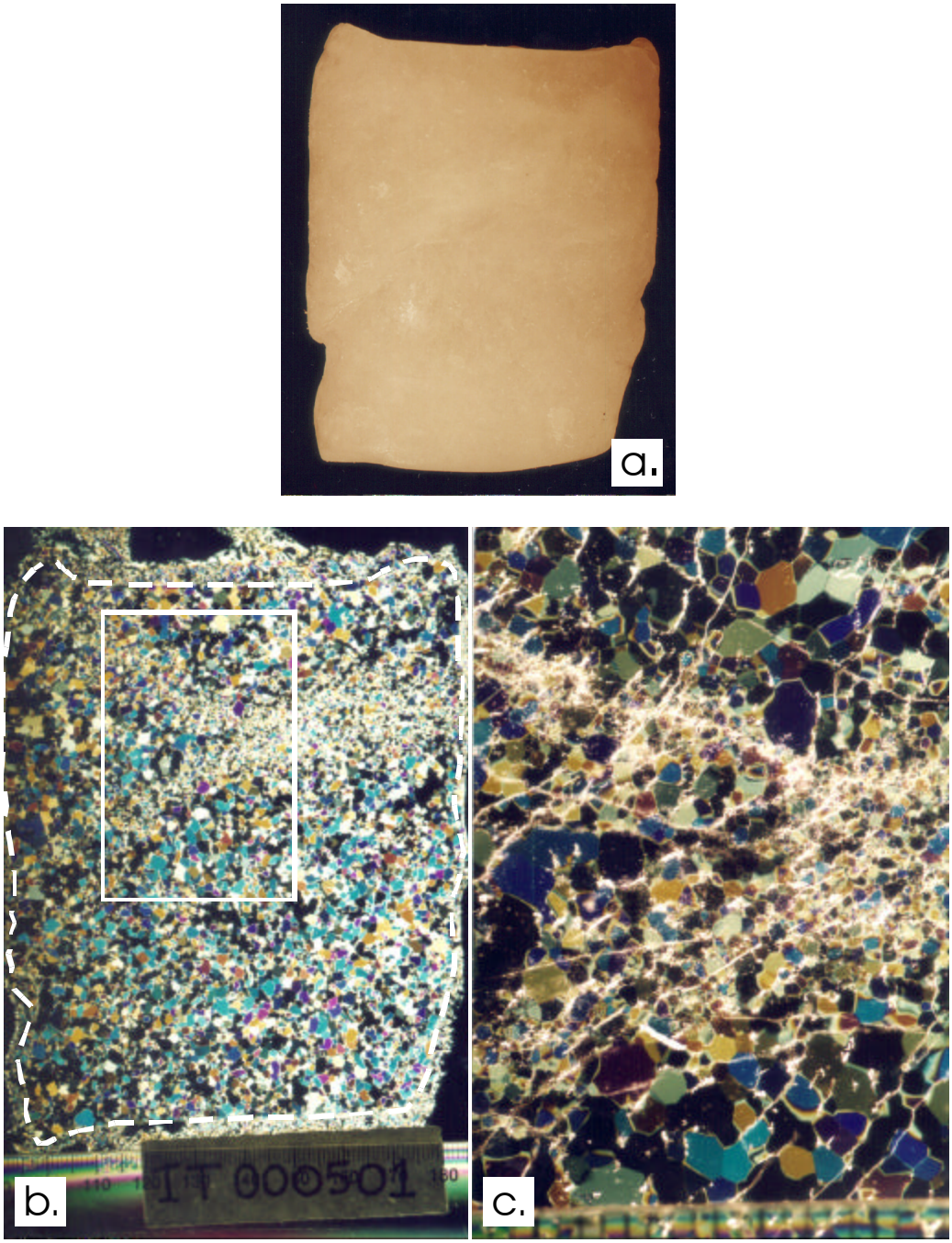

Figure 25: (a) Specimen of iceberg ice deformed to 31% true strain at a confinement of 50 MPa, -10 ^{o}C.. (b) Thin section of whole specimen showing grain refinement along planar zones. (c) Enlarged view of (b) with side (reflected) light, showing the nature of the grain refinement. It consists of new crystals but where fracturing is also present. Scale in mm.

Figure 26: Ice specimen from laboratory-produced ice tested at high confinement. The pencil can be seen through the ice, a feature that is characteristic of strongly recrystallized ice that displays very little microcracking. The lighter zone near the upper surface is caused by the presence of air entrapment in the specimen before deformation.

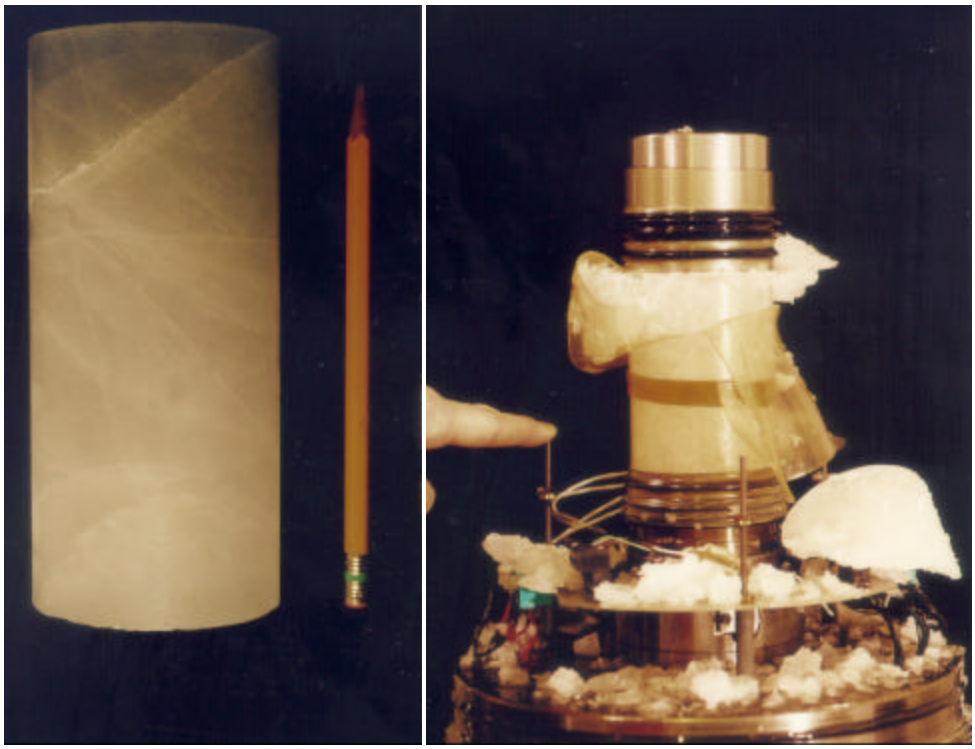

Figure 27: Example of an unsuccessful test. A planar 'flaw' near the top end of the specimen (left) was unable to withstand the axial load on the specimen, leading to immediate collapse. The minimum strain rate was not attained and no data resulted from this test. Pencil and finger for scale.

Appendix 3

Data Tables

LABORATORY ICE						
test #	Conf. (MPa)	Axial stress (MPa)	Pressure (MPa)	Temperature (^{o}C)	Non-Corrected Minimum Strain rate ln(sec^{-1})	Corrected Minimum Strain rate(*) ln(sec^{-1})
i010531	30	15	35	-10.8	-7.15	-7.10
i010528	65	15	70	-9.5	-5.85	-5.80
i010525	65	15	70	-18.0	-8.30	-8.25
i010524	60	15	65	-16.8	-8.10	-8.10
i010523	60	15	65	-11.8	-8.20	-8.15
i010510	50	15	55	-9.6	-6.95	-6.90
i010509	30	15	35	-11.4	-7.30	-7.24
i010425	30	15	35	-21.4	-8.80	-8.38
i010307	60	15	65	-20.3	-8.85	-8.80
i010306	10	15	15	-9.7	-7.32	-7.30
i010305	10	15	15	-26.7	-9.40	-9.35
i010303	65	15	70	-25.0	-9.50	-9.45
i010302	60	15	65	-25.3	-9.45	-9.40
i010229	50	15	55	-20.6	-8.65	-8.60
i010227	50	15	55	-16.6	-8.40	-8.25
i010226	50	15	55	-11.6	-7.70	-7.68
i010223	10	15	15	-6.7	-6.57	-6.54
i010222	60	15	65	-15.3	-8.04	-8.00
i010221	65	15	70	-24.0	-8.50	-8.45
i010220	60	15	65	-24.3	-8.90	-8.80
i010219	60	15	65	-18.3	-9.14	-9.10
i010215	65	15	70	-20.0	-8.94	-8.90
i010113	65	15	70	-8.5	-5.40	-5.35
i001031	65	15	70	-14.0	-7.75	-7.65
i001026	65	15	70	-9.3	-5.20	-5.15
i000908	10	15	15	-20.7	-8.52	-8.50
i000906	10	15	15	-10.7	-7.30	-7.35
i000630	60	15	65	-9.3	-5.70	-5.40
i000623	50	15	55	-24.6	-9.35	-9.15
i000621	30	15	35	-24.4	-9.65	-9.60
i000619	10	15	15	-15.7	-7.90	-8.00

i000616	10	15	15	-5.5	-6.01	-5.90
i000614	30	15	35	-15.4	-8.85	-8.80
i000612	50	15	55	-4.6	-6.10	-6.10
i000609	30	15	35	-5.4	-6.80	-6.65
i000313	50	15	55	-13.6	-8.39	-8.35
i000308	50	15	55	-10.6	-8.55	-8.45

ICEBERG ICE

test #	Conf. (MPa)	Axial stress (MPa)	Pressure (MPa)	Temperature (^{o}C)	Non-Corrected Minimum Strain rate ln(sec^{-1})	Corrected Minimum Strain rate(*) ln(sec^{-1})
i010623	65	15	70	-25.0	-7.90	-7.80
i010622	50	15	55	-25.0	-7.40	-7.20
i010621	10	15	15	-25.0	-8.60	-8.35
i010620	60	15	65	-20.0	-8.30	-8.20
i010616	50	15	55	-20.0	-7.10	-7.00
i010615	65	15	70	-20.0	-6.90	-6.80
i010614	30	15	35	-26.0	-7.40	-7.30
i010613	10	15	15	-16.0	-6.70	-6.85
i010612	60	15	65	-15.5	-7.30	-7.20
i010608	30	15	35	-19	-6.65	-6.60
i010507	50	15	55	-14.6	-7.20	-7.30
i010501	10	15	15	-6.2	-5.76	-5.75
i010427	65	15	70	-14.0	-7.05	-7.00
i010426	10	15	15	-10.7	-5.18	-5.16
i010420	60	15	65	-11.3	-6.41	-6.40
i010216	65	15	70	-10.0	-5.06	-5.03
i010213	30	15	35	-10.6	-7.10	-7.00
i000501	50	15	55	-8.6	-6.40	-6.25

(*) The correction was to remove the effect of 'barelling' in the specimen (keeping in mind that the tests were done under constant load, not constant stress). This correction is approximate and was done by assuming a constant volume for a widening, but straight-sided, cylinder and determining the increase in diameter for each increment of axial strain. The effective stress was then obtained by dividing the load applied to the specimen by this new area. The minimum strain rate was then increased correspondingly using Glen's law and a stress exponent of 4. This resulted in the rate shown in this column. The correction is minimal, however, and could probably be ignored for the small amount of strain (about 1%) required to reach the minimum strain rate.